Supplementary Information

Phosphine-based Metal-Organic Layers to Construct Single-Site Heterogeneous Catalysts for Arene Borylation

Content

1. Materials and methods

All reagents were commercially available and used without further purification unless otherwise stated. N, N-Dimethylformamide (DMF), formic acid (HCO_2H) and H_2O were removed dissolved oxygen by bubbling nitrogen (N_2). Tetrahydrofuran (THF) and toluene was distilled prior to use. The resistance vials with PTFE lined caps were purchased from WHEATON (USA).

Powder X-ray diffraction (PXRD) patterns were performed on Rigaku IV diffractometer with Cu Kα radiation (λ = 1.54178 Å). Transmission electron microscopy (TEM) images were recorded on a JEOL JEM-1400 (120kV). High-resolution transmission electron microscopy (HRTEM) and high-angle annular dark field (HAADF) images were acquired in Tecnai F30 scanning transmission electron microscopy (STEM, Philips-FEI) operated at 300 kV. Atomic force microscopy (AFM) images were collected by Cypher S Asylum Research atomic force microscopy using tapping mode. Thermogravimetric analysis (TGA) was measured by a Shimadzu TGA-50 in air equipped with an alumina pan and heated at a rate of 10 °C per minute. ^{1}H-NMR, ^{31}P-NMR and ^{13}C-NMR spectra were recorded on a Bruker 400 DRX spectrometer at 400 MHz and a Bruker 500 DRX spectrometer at 500 MHz. The D1 relaxation delay was set to 30 s for ^{1}H-NMR quantification of HCO_2^- and TPP. N_2 sorption isotherm was performed measured on a Micrometrics ASAP 2040 instrument at 77 K. Inductively coupled plasma-optical emission spectroscopy (ICP-OES) data were obtained from a Thermo Fisher iCap 7000 instrument. Gas chromatography-mass spectrometry (GC-MS) was performed on a Shimadzu QP2010 Plus spectrometer for all analyses of interest. X-ray photoelectron spectroscopy (XPS) were measured on a Thermo Fisher spectrometer. The binding energy was corrected by the C 1s peak (284.8 eV). High-resolution mass spectra were measured by Agilent 1290-6545XT quadrupole TOF mass spectrometry with an electrospray ionization (ESI) source.

2. Synthesis of TPP ligand

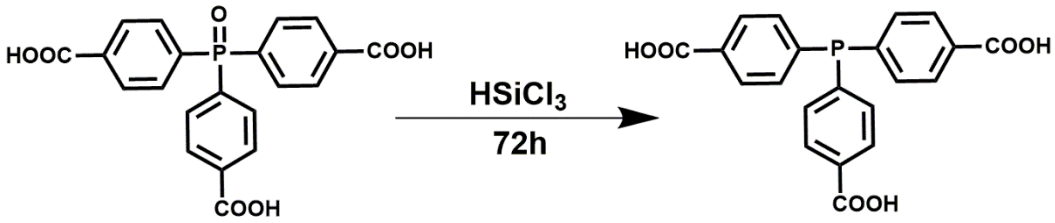

Fig. S1 Synthesis of TPP ligand.

The synthesis of Tris(4-carboxylphenyl)phosphine oxide (TPO) followed the reported literature.[1,2] The obtained TPO (2g, 4.9 mmol) was suspended in anhydrous toluene (34 mL) in a 250 mL schlenk tube. The reducing agent $HSiCl_3$ (22 mL, 218 mmol) was added. The suspension was heated at 130 °C for 3 days under nitrogen atmosphere. Afterward, the solvent were removed via evaporation. The concentrated NH_3 solution was added to the yellow residue and the aqueous phase containing the product was separated by centrifugation. The filtrate was acidified with dilute HCl to obtain a white solid. The collected solid was washed with deionized water and dried at 60 °C under vacuum to give the TPP ligand as a white powder (1.23 g, 64%).

^{1}H NMR (500 MHz, DMSO-d_6) δ 13.13 (s, 3H), 7.97 (dd, J = 8.3, 1.6 Hz, 6H), 7.39 (t, J = 7.8 Hz, 6H).

^{13}C NMR (126 MHz, DMSO-d_6) δ 167.00 , 140.99 (d, J = 13.6 Hz), 133.52 (d, J = 19.8 Hz), 131.74 , 129.67 (d, J = 7.0 Hz).

^{31}P NMR (202 MHz, DMSO-d_6) δ -6.37.

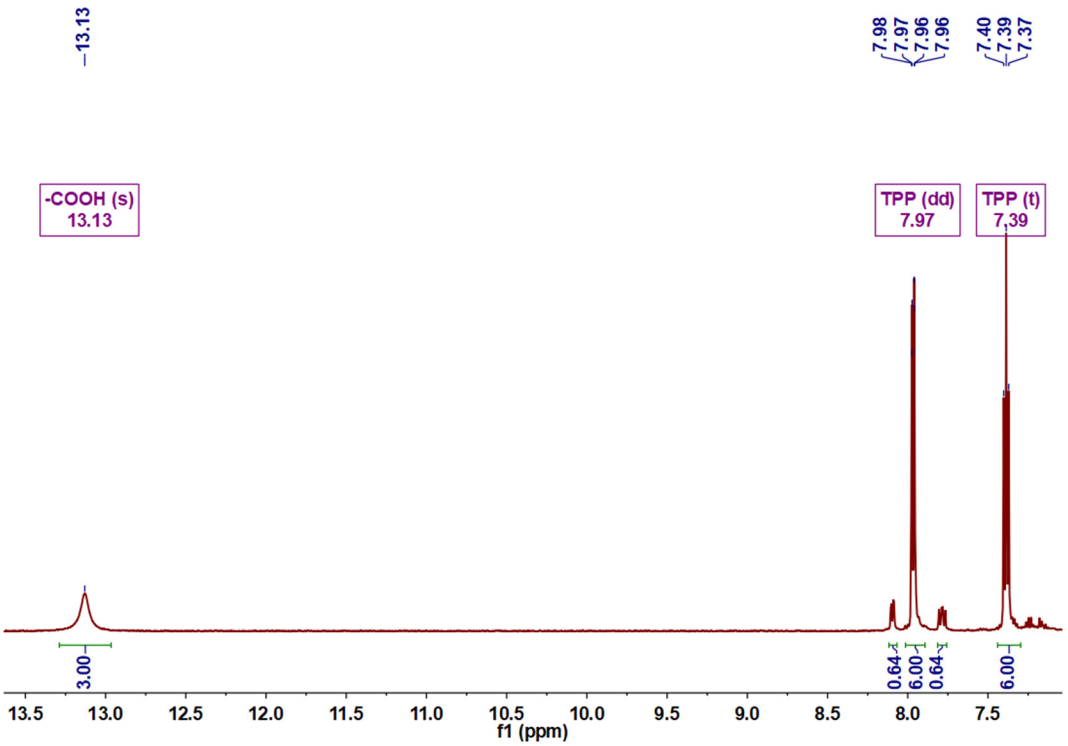

Fig. S2 ^{1}H-NMR spectrum of TPP ligand in DMSO-*d*$_6$ (500 MHz). The proportion of the unreduced TPO accounts for less than 10% in the resulting ligand. Due to the similarity of the two ligands, a small amount of TPO ligand is feasible to grow into the TPP-MOL, leading to local disorder of the structure.

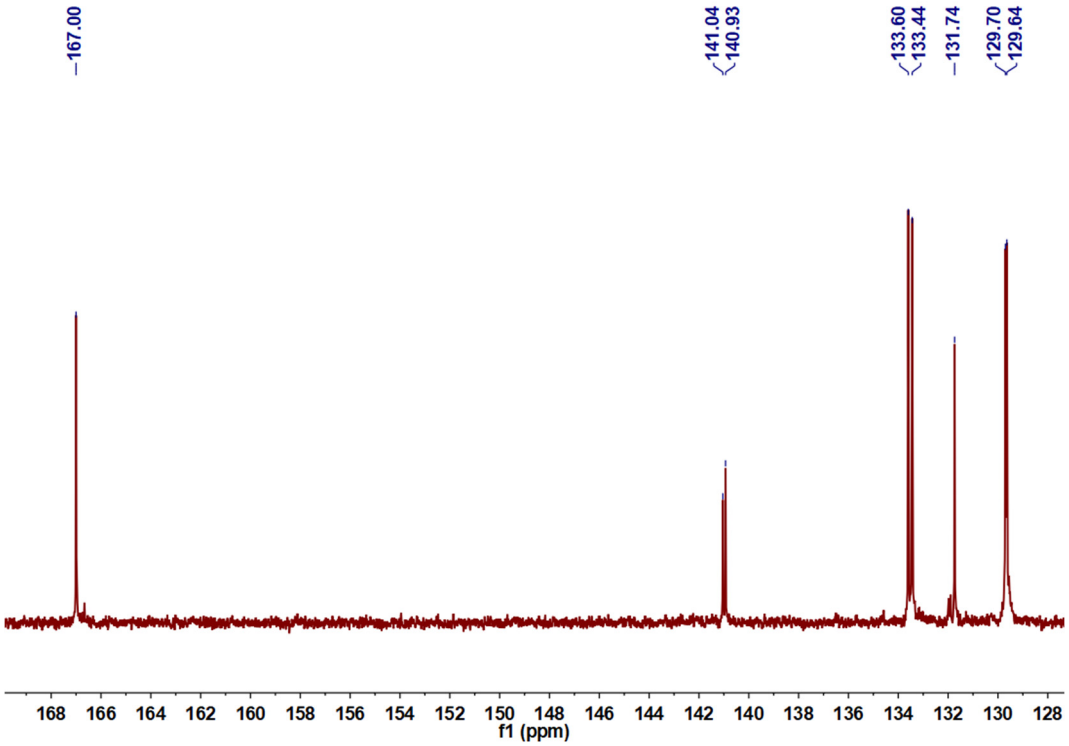

Fig. S3 ^{13}C-NMR spectrum of TPP ligand in DMSO-*d*$_6$ (126 MHz).

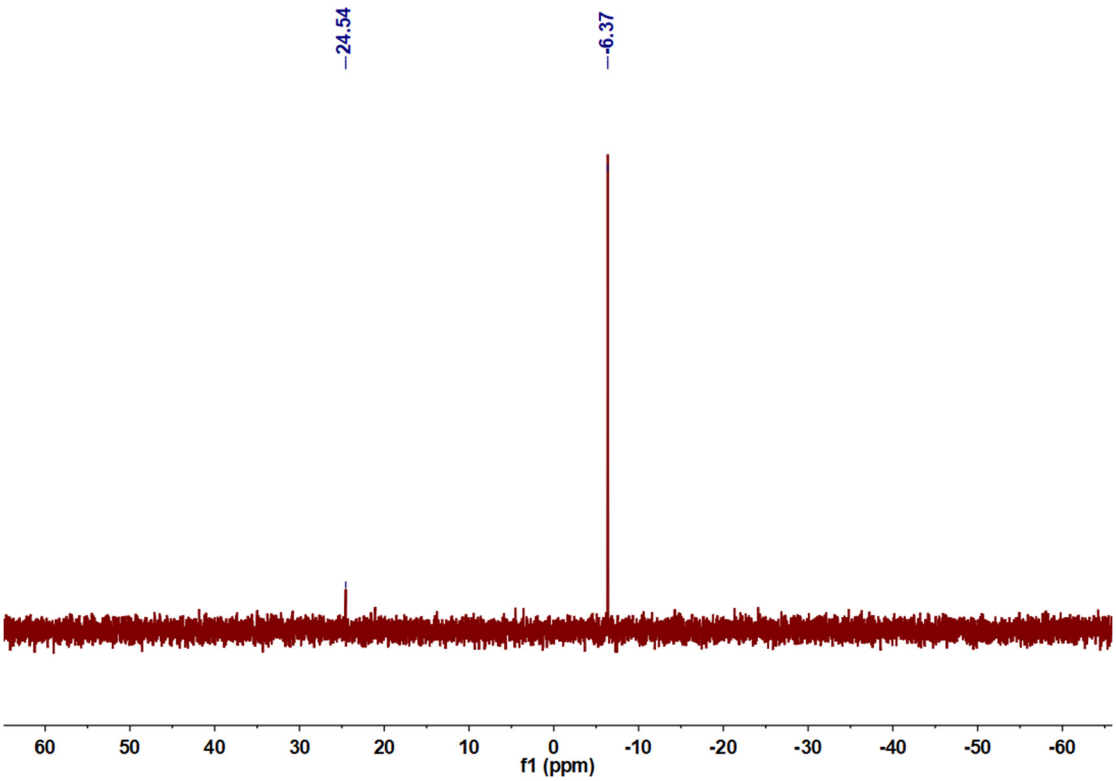

Fig. S4 ^{31}P-NMR spectrum of TPP ligand in DMSO-d_6 (202 MHz).

3. Structure of Zr_6 SBU in a single layer exfoliated from TPO-MOF

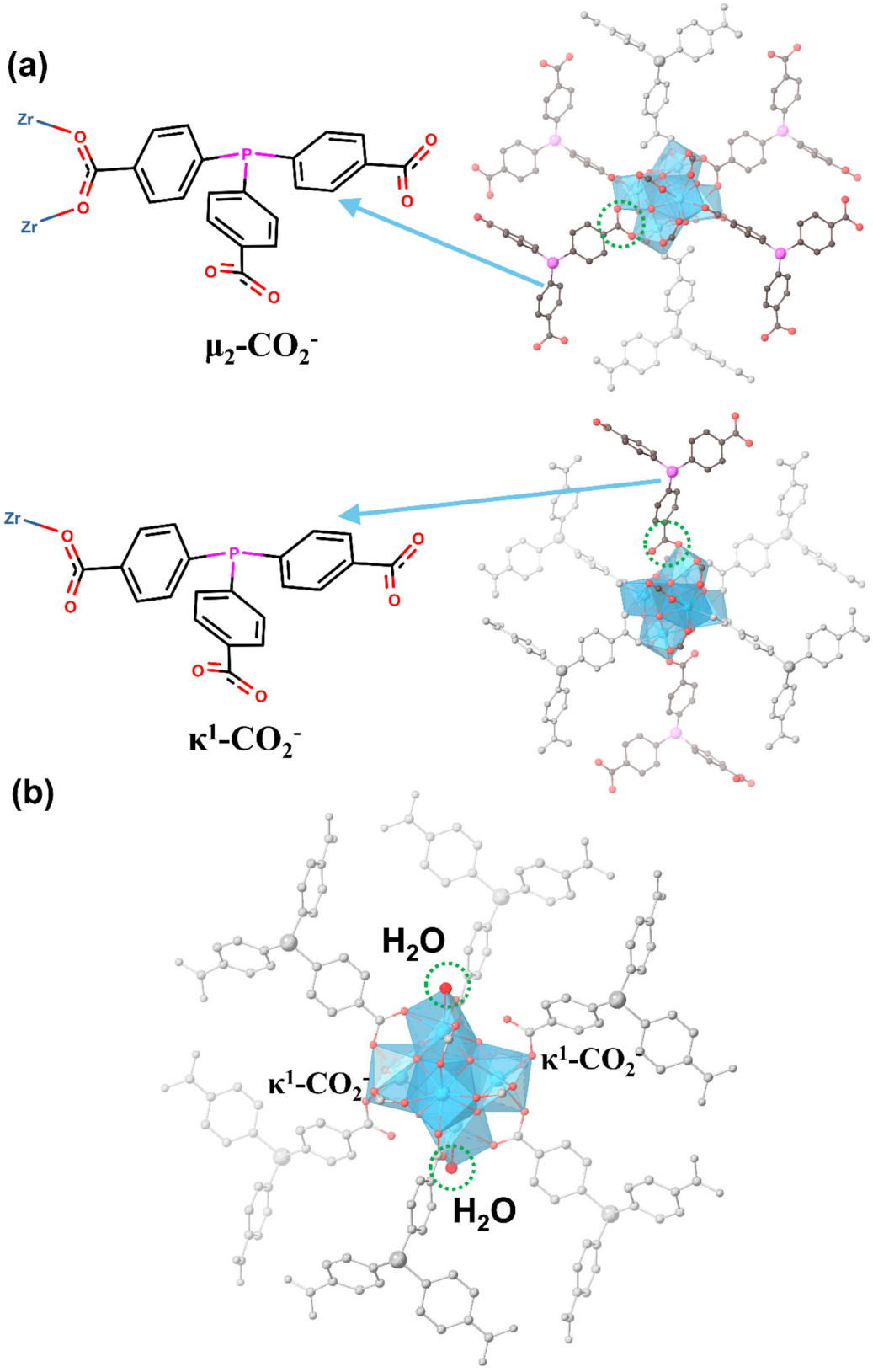

Fig. S5 Structure of Zr_6 SBU in a single layer exfoliated from TPO-MOF. (a) Two modes of coordination to metals of CO_2^- (μ_2-CO_2^- and κ^1-CO_2^-). (b) Zr^{4+} coordination in the κ^1-CO_2^- mode supplemented by oxygen on H_2O.

4. Synthetic conditions of 2D TPP-MOL

Synthesis of 2D TPP-MOL

The synthetic procedure was carried out under N_2 protection using a glove box. The synthetic conditions of TPP-MOL were optimized though systematically regulating the amount of HCO_2H. As shown in Fig. S5 and S6, the samples transitioned from amorphous phase to 2D MOL, and then transformed into 3D MOF as increasing the amount of HCO_2H. The introduction of HCO_2H in the synthesis of MOL can act as a capping molecule to deduce the surface energy and a coordination regulatory species. The introduction of HCO_2H in the synthesis of MOL can act as a capping molecule. Increasing the amount of HCO_2H results in a completely capped surface that is beneficial for packing between layers. The 2D MOL can then pack into the 3D MOF. This phenomenon is not uncommon in MOL synthesis[3]. The optimal MOL production condition is usually with partially capped MOL surface so that the surface irregularity makes packing between layers energetically unfavorable.

For the typical synthesis of TPP-MOL, $HfCl_4$ (12 mg, 0.038 mmol) and TPP (11.7 mg, 0.03 mmol) were dissolved in a solution of 0.833 mL of DMF and 0.025 mL of H_2O, 0.12 mL of HCO_2H was added into the reaction mixture. The pressure-resistance vial was sealed and heated at 120 °C for 2 days under N_2 protection. After cooling down to room temperature, the white precipitates were obtained by centrifugation and washed with DMF and acetonitrile more than 3 times.

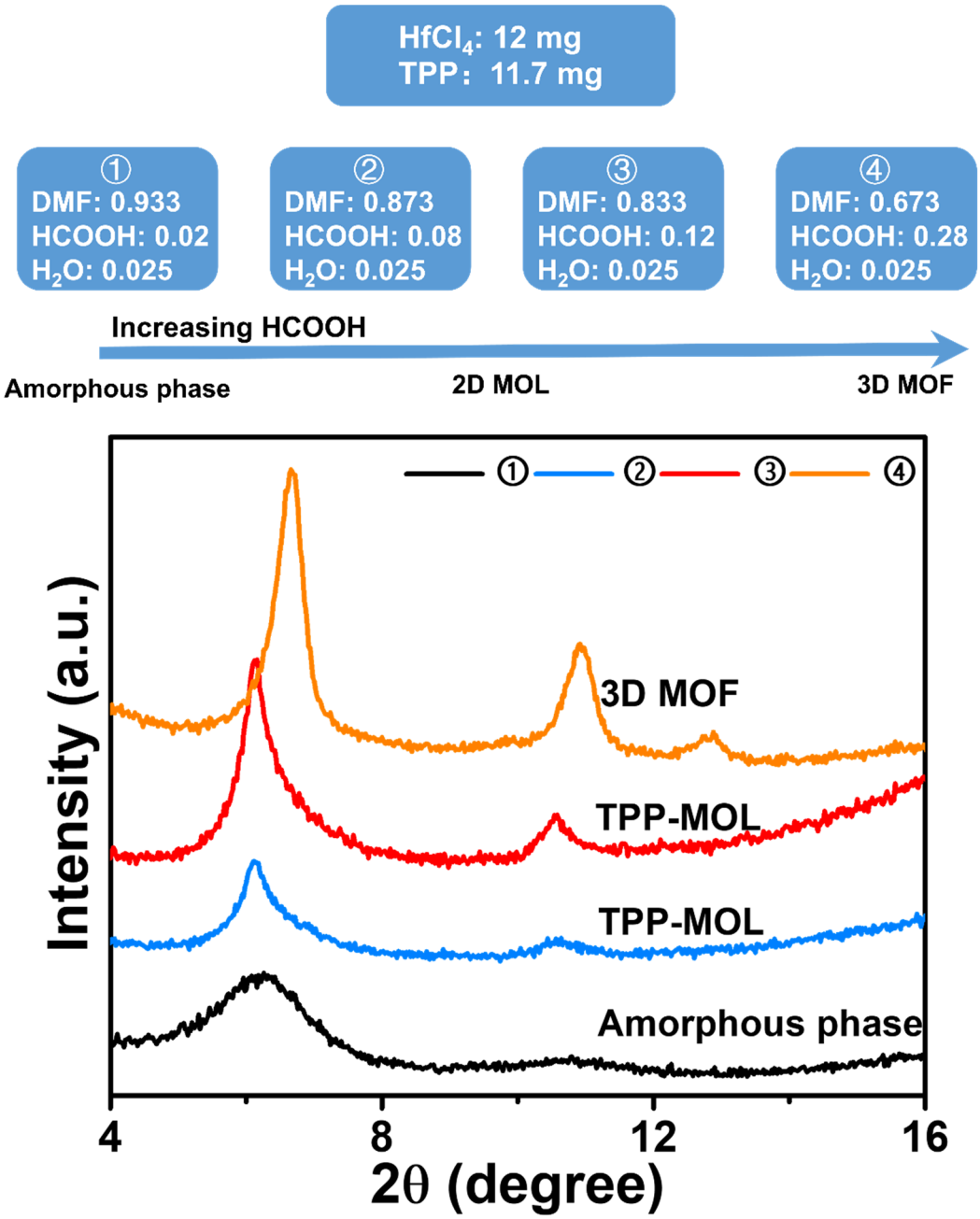

Fig. S6 PXRD patterns of samples synthesized with different amount of HCO_2H (in mL) at 120 °C for 2 days.

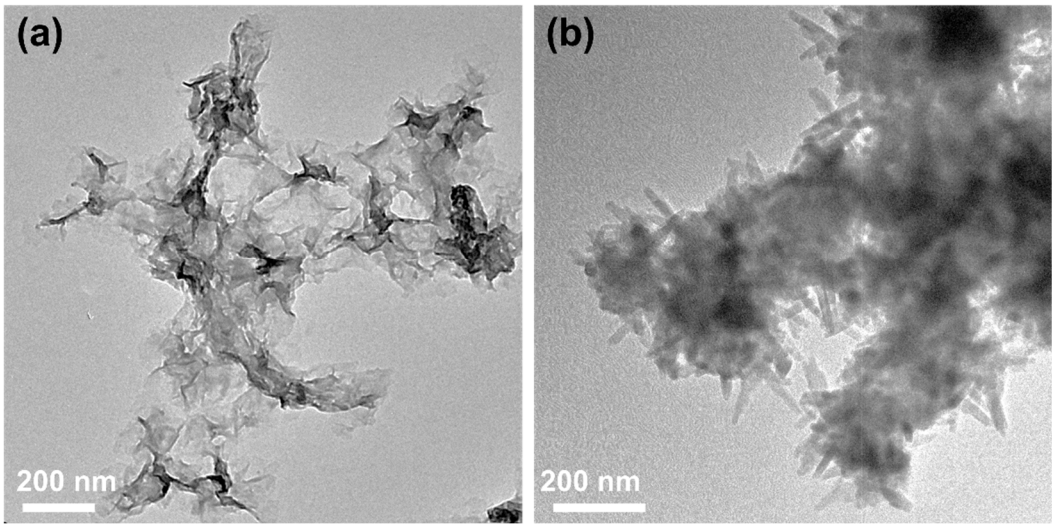

Fig. S7 TEM images of (a) 2D TPP-MOL and (b) 3D MOF.

5. Structure of TPP-MOL

To determine the structure model of the TPP-MOL, the optimized synthetic conditions was screened to improve the crystallization. And then high-resolution transmission electron microscopy was carried out more times, but TEM images were with a well-defined arrangement of SBUs were not obtained. It was also found that the MOL underwent beam radiation damage, making it difficult to capture clearer images.

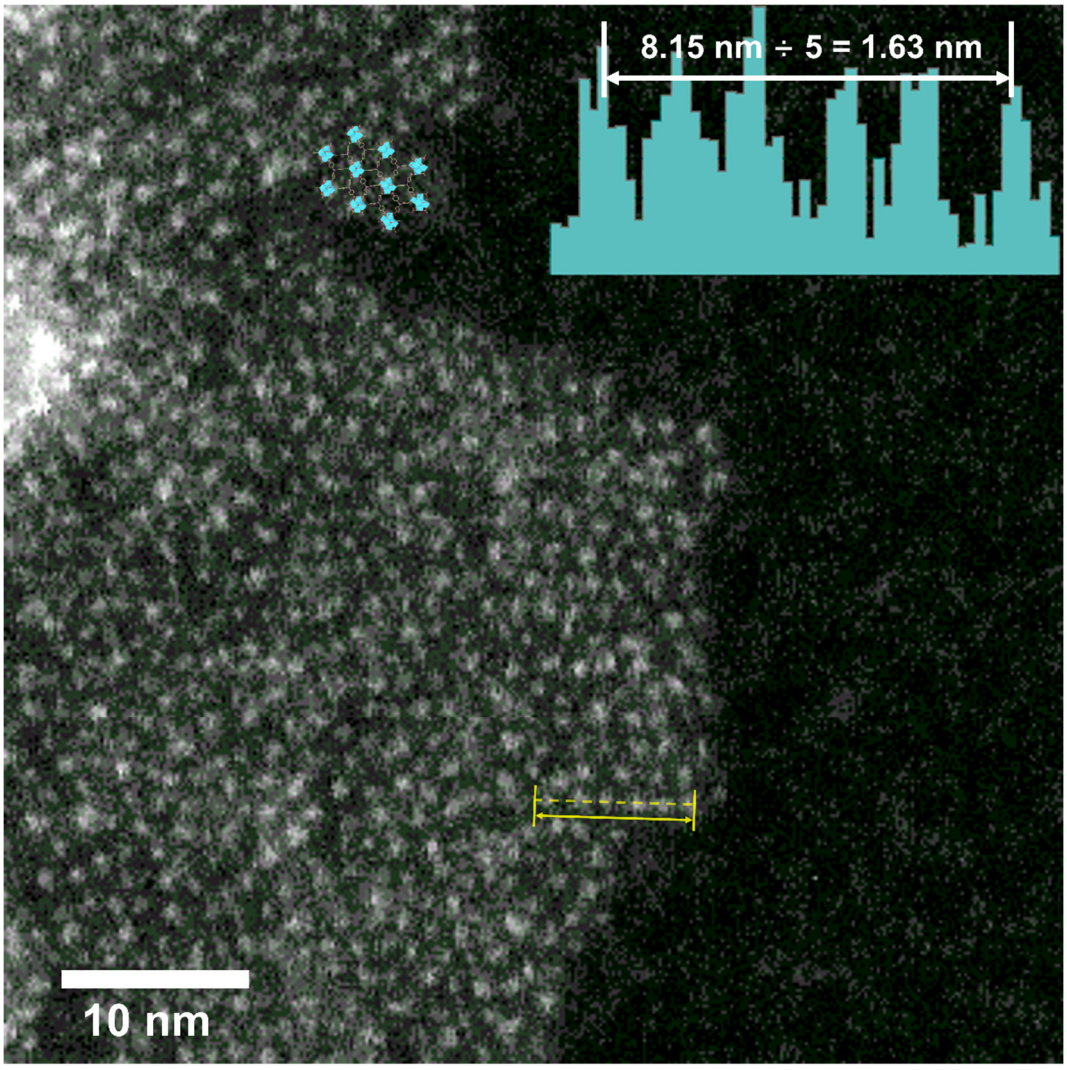

Fig. S8 HADDF image of TPP-MOL. As shown in the image, the spacing between adjacent SBUs in the HADDF image was 16.6 ± 0.5 Å.

6. Structure construction and PXRD simulation of TPP-MOL

The structural model of TPP-MOL was constructed by using Materials Studio 2017 software based on the information of the unit cell and Hf_6-oxo distribution as well as related crystal structure. The Bragg equation describing 3D crystal

diffraction is not applicable to 2D materials due to the finite repeats in the third dimension. Based on this, our group developed the simulation method for PXRD patterns of 2D materials using a complete integration method in real space (CIREALS). The simulated PXRD pattern of TPP-MOL was acquired by a developed Matlab codes taking a CIF files as structural input (https://github.com/Wang-Group/2D-XRD-Modelling)[4]. As shown in Fig. 2c, the peaks of experiment and simulation PXRD pattern of TPP-MOL are not symmetrical Gaussian profile: the diffraction intensity rises rapidly on the low-angle side and decreases slowly on the high-angle side. This is a characteristic PXRD peak profile of the ultrathin material and can be well explained theoretically, indicating that TPP-MOL is very thin with a single layer or a few layers[3, 4].

7. Analysis of chemical composition for TPP-MOL

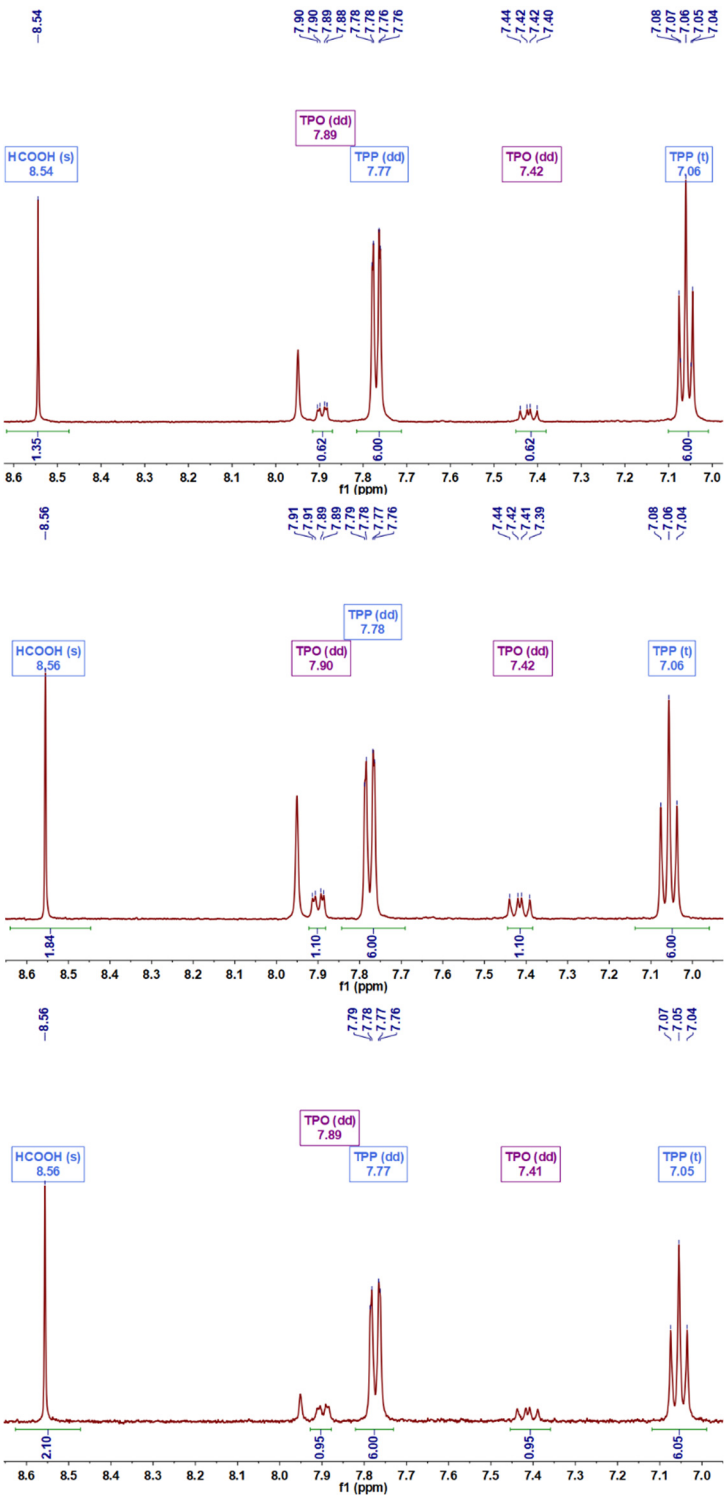

Fig. S9 ^{1}H-NMR spectra of the digested TPP-MOL by tetra-n-butylammonium fluoride (TBAF) for three repeated experiments. The measured formate/ligand ratio by ^{1}H-NMR quantification is 1.5 ± 0.3, where the ligand is defined to be the sum of the amounts of TPP and oxidized-state TPO (9% to 15%).

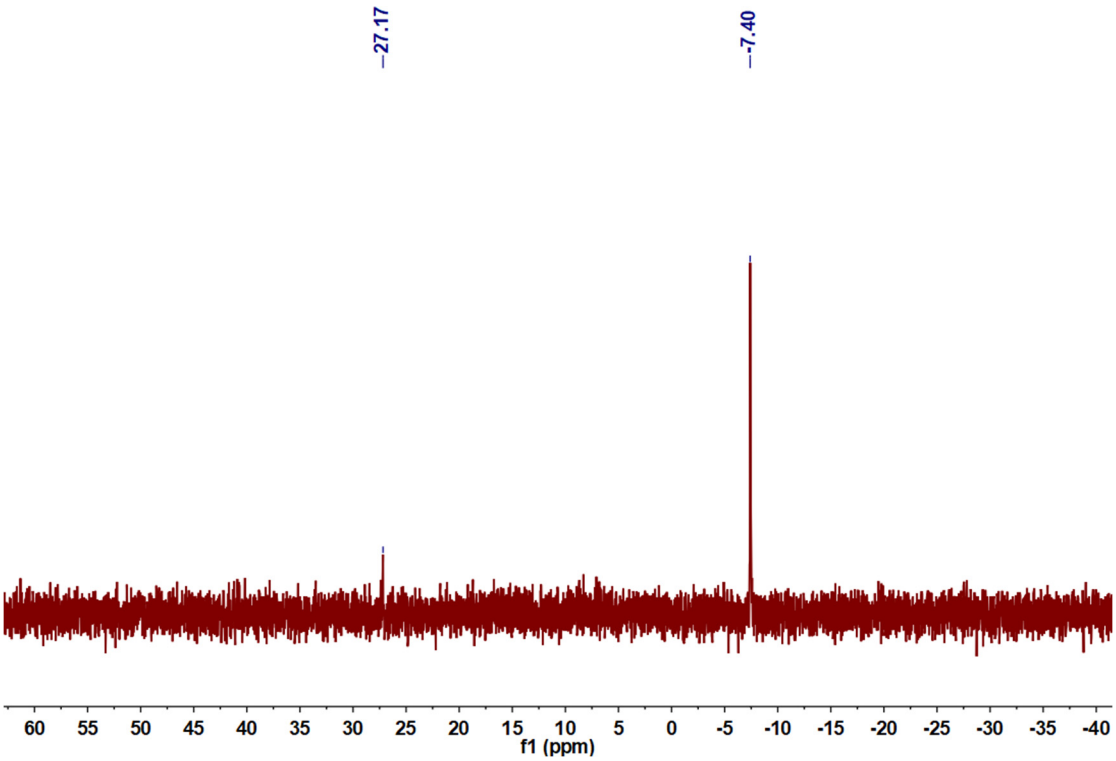

Fig. S10 ^{31}P-NMR spectrum of the digested TPP-MOL by TBAF.

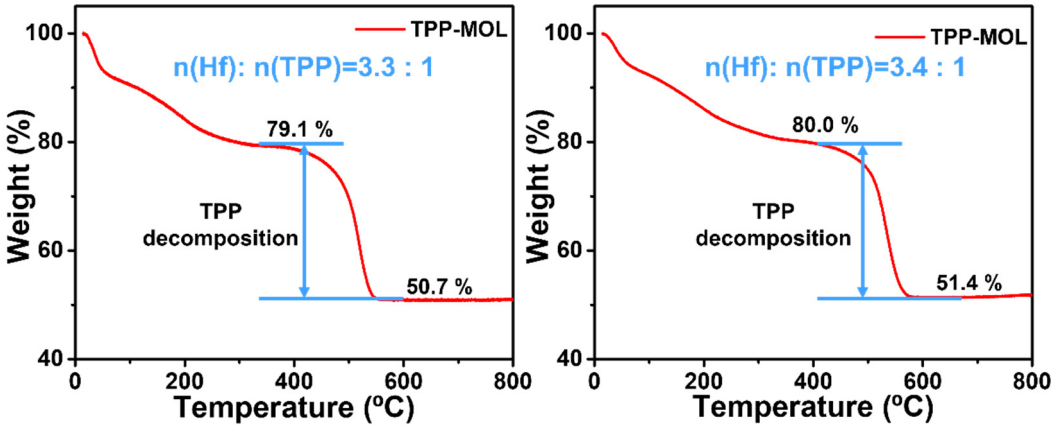

Fig. S11 TGA plots of TPP-MOL (two repeated tests). The average molar ratio of Hf : TPP is 3.35.

8. Synthesis and structure of 3D TPP-MOF

$Zr_{12}O_8(OH)_8(CH_3CO_2)_{24}$ cluster was synthesized following the procedure reported in the literature.[5, 6] TPP (16.0 mg, 0.04 mmol) was dissolved in 1.4 mL DMF in an 8 mL vial. 2.12 ml of acetic acid (CH_3CO_2H) was added into the mixed solution. After stirring for 5 minutes, $Zr_{12}O_8(OH)_8(CH_3CO_2)_{24}$ cluster (55.6 mg, 0.018 mmol) was added to the reaction system. Under N_2 atmosphere, the vial was sealed with a PTFE lined cap and heating in an oven at 120 °C for 3 days. The white powder was collected and washed with DMF and acetonitrile.

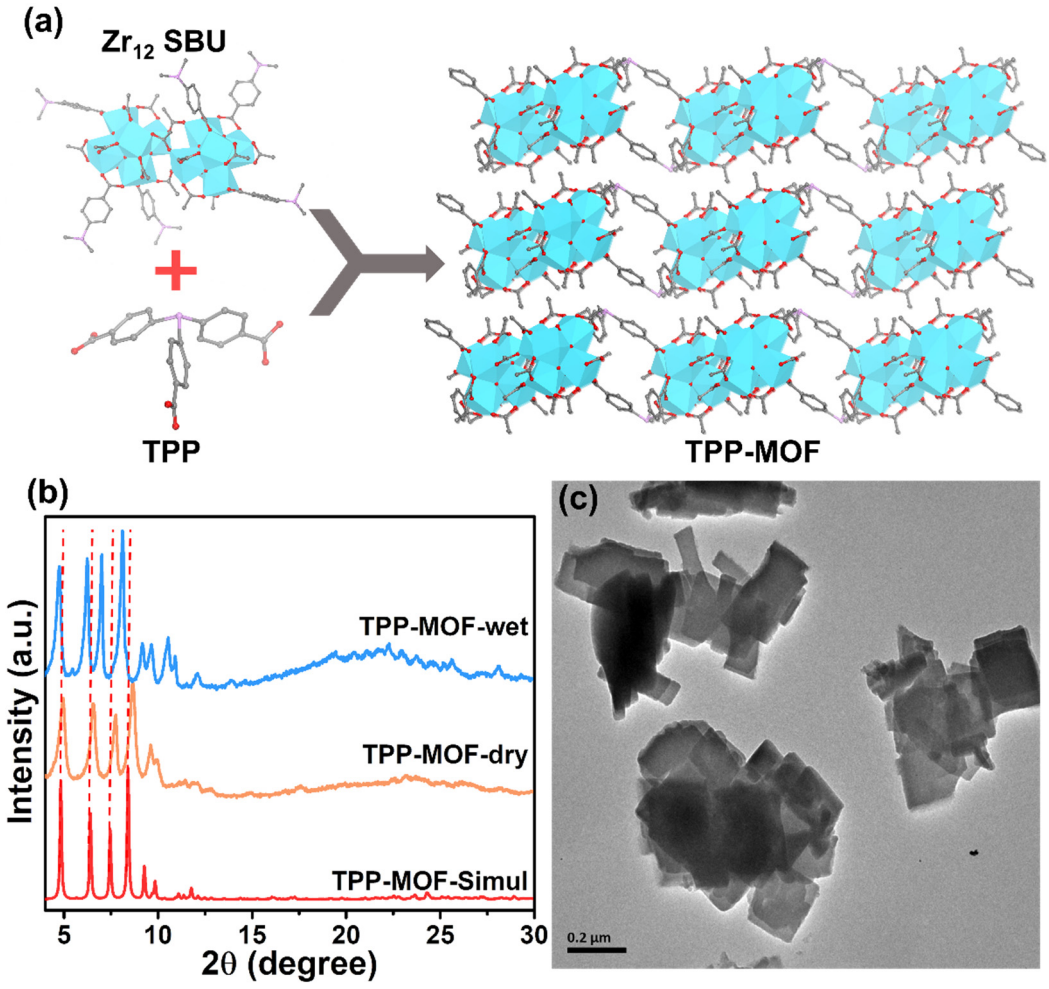

Fig.S12 (a) Structure of 3D TPP-MOF. (b) PXRD patterns and (c) TEM image of 3D TPP-MOF. The diffraction peaks of TPP-MOF in wet state shifted to smaller angle compared to the simulated pattern from the TPP-MOF crystal, while the dry sample did the opposite. The phenomenon can be well understood by the breath effect resulting from the solvent within the framework.

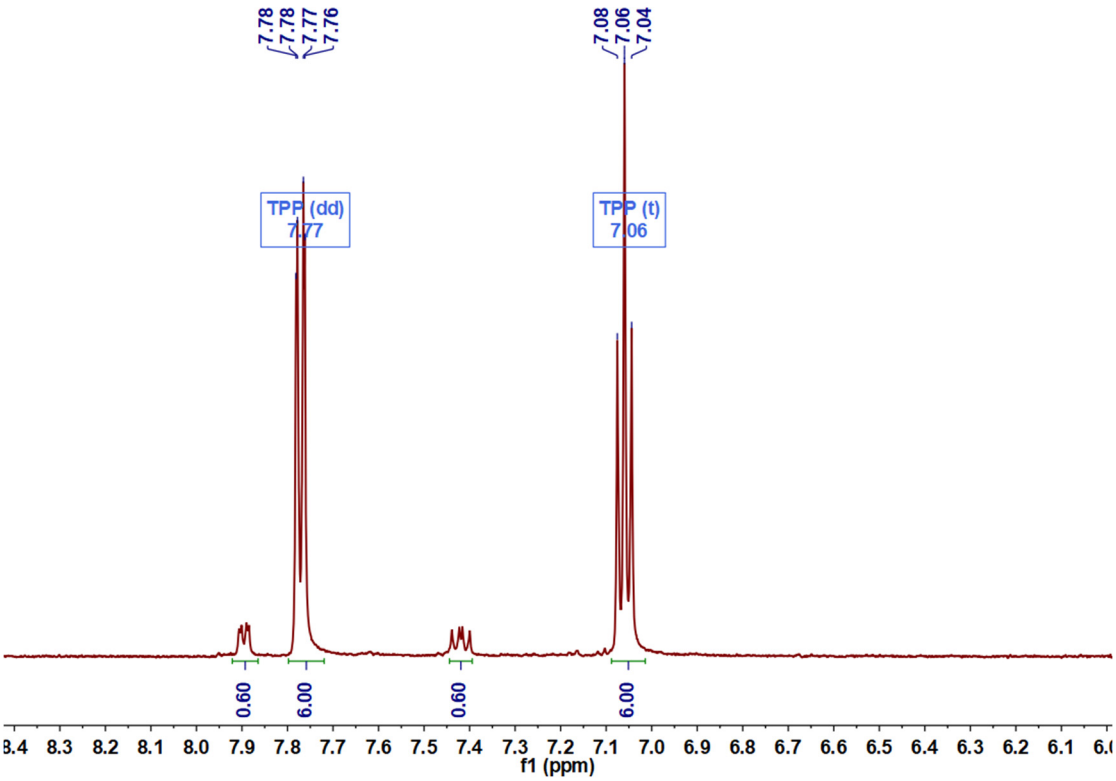

Fig.S13 ^{1}H-NMR spectrum of the digested TPP-MOF by tetra-n-butylammonium fluoride (TBAF).

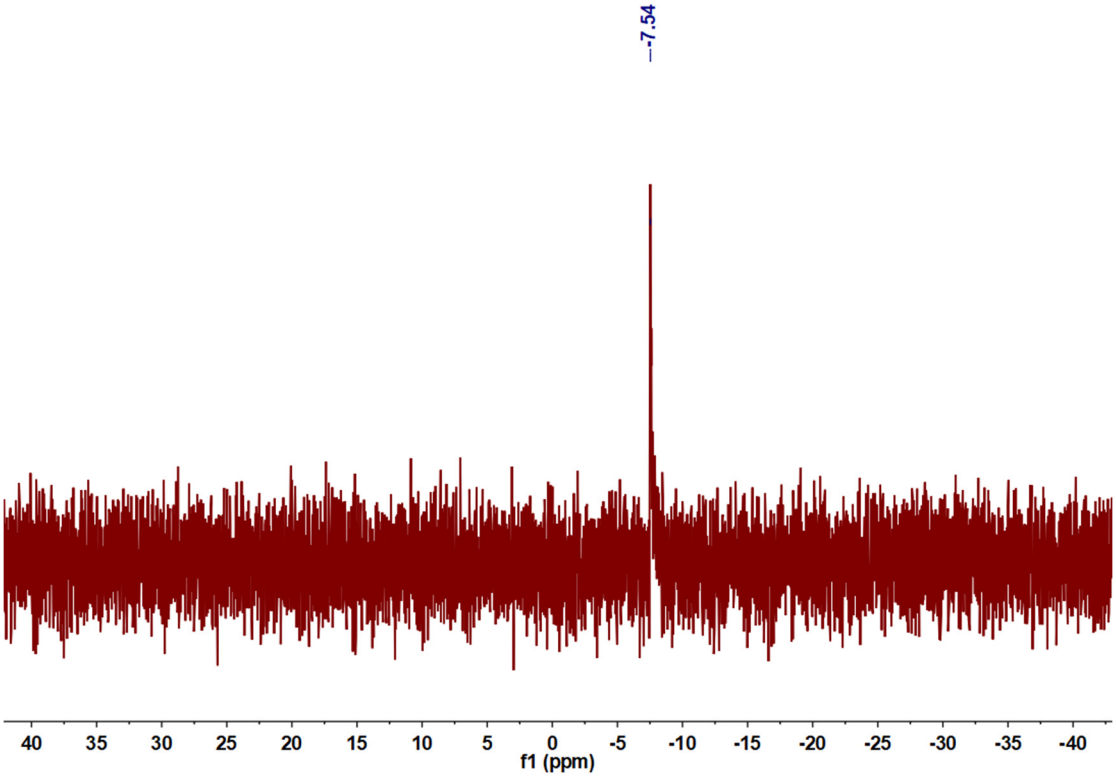

Fig. S14 ^{31}P-NMR spectrum of the digested TPP-MOF by tetra-n-butylammonium fluoride (TBAF).

9. General procedures for catalytic borylation

Synthesis of TPP-MOL-Ir Catalyst

The TPP-MOL (3 μmol P) was dispersed in 2 mL acetonitrile and transferred into glove box. $[Ir(COD)Cl]_2$ (5 mg, 7.5 mmol) was added and stirred overnight at room temperature. The postsynthetically metallized TPP-MOL was centrifuged from the suspension and washed 5 times with acetonitrile and THF. ICP-OES analysis showed that 0.27 μmol of Ir-loading amount was obtained and the P/Ir ratio of the load was 1 : 0.9. As for the catalyst loading of 0.54 mol%, the amount of P (3 μmol) used in each reaction was quantitatively tested by ^{1}H-NMR results. Then, the loading of Ir (90%) can be confirmed by ICP-OES data and the content of Ir (0.27 μmol) in the TPP-MOL-Ir can be calculated. The catalytic equivalent ratio of Ir (0.54 mol%) can be given by dividing the Ir content by the feeding amount of B_2pin_2 (0.5 mmol).

As control catalysts, TPP-Ir as a homogeneous catalyst was prepared by triphenylphosphine (PPh_3) metallized with equal amounts of $[Ir(COD)Cl]_2$ (Table S1, Entry 9). 3D TPP-MOF was metallized with $[Ir(COD)Cl]_2$ under same condition, the P/Ir ratio of the load was 7 : 1 due to the limitation of channels (Table S1, Entry 10).

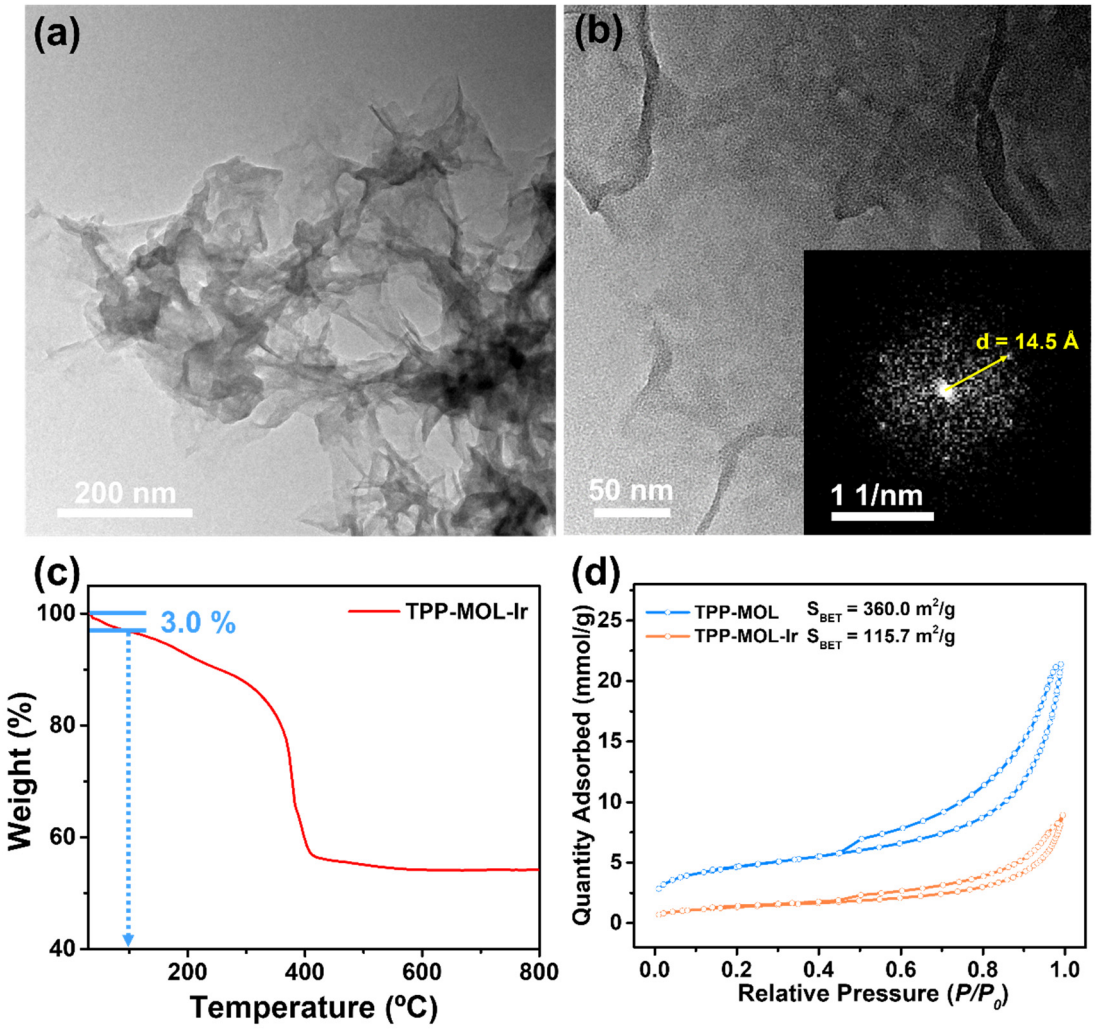

Fig. S15 (a, b) TEM images of TPP-MOL-Ir. The inset in the b is the FFT diffraction pattern. (c) TGA plot of TPP-MOL-Ir. (d) Nitrogen sorption isotherm of TPP-MOL and TPP-MOL-Ir.

General procedure for the aromatic C-H borylation

The wet TPP-MOL-Ir catalyst (3 μmol P) or other catalysts, bis(pinacolate)diborane (B_2pin_2, 127 mg, 0.5 mmol), arenes (2 ml) were added into a 25 ml schlenk tube in the glovebox. The reactants were gently stirred at 100 ℃ for 24 h. After cooling to room temperature, TPP-MOL-Ir/TPP-MOF-Ir was filtered by centrifugation and the supernatant was tested by ^{1}H-NMR (mesitylene as an internal standard) and GC-MS to determine the yield and selectivity for borylation product. The yield and TON of C_6H_4RBpin for each reaction were calculated as follow.

$$\text{Yield } C_6H_4RBpin\% = \frac{n_{C_6H_4RBpin}\ (mol)}{n_{B_2pin_2}\ (mol)} \times 100\%$$

$$TON = \frac{B_2pin_2\ (mol) \times C_6H_4RBpin\ \text{yield}\ (\%)}{\text{Loading Ir}\ (mol)}$$

More than 100% yield is attributed to some reactivity between TPP-MOL-Ir catalyst and HBpin byproduct during the borylation reaction[7].

Effects of temperature and the amount of B_2pin_2 and contrast experiment

When the amount of B_2pin_2 is 0.15 mmol with too high a catalyst loading, changing the reaction temperature from 60 °C to 100 °C (Table S1, Entry 1-3) did not significantly affect the yield with a high conversion. Increasing the amount of B_2pin_2 to 0.5 mmol showed a much higher yield. The TPP-MOL-Ir catalyst achieved the highest yield of 98.9% at 100 °C. The decrease in temperature resulted in an incomplete conversion of B_2pin_2 and a drop in $C_6H_4ClBpin$ yield (Table S1, Entry 4-6). Moreover, when the amount of B_2pin_2 was increased to 1 mmol, the TPP-MOL-Ir catalyst showed similar TON with 0.5 mmol of B_2pin_2 addition at 100 °C (Table S1, Entry 7).

Table S1.TPP-MOL-Ir catalyzed C(sp^2)–H borylation of chlorobenzene.[a]

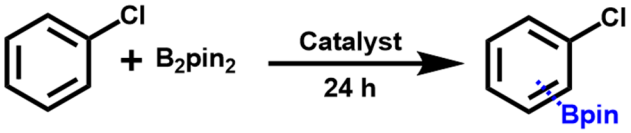

Entry	Catalyst	Temp (°C)	Yield of $C_6H_4ClBpin$ (%)[b]	TON
1	1.8 mol% TPP-MOL-Ir[c]	60	94.5	-
2	1.8 mol% TPP-MOL-Ir[c]	80	93.8	-
3	1.8 mol% TPP-MOL-Ir[c]	100	96.3	-
4	0.54 mol% TPP-MOL-Ir	60	47.7	88
5	0.54 mol% TPP-MOL-Ir	80	70.1	130
6	0.54 mol% TPP-MOL-Ir	100	98.9	183
7	0.27 mol% TPP-MOL-Ir[d]	100	49.8	184
8	TPP-MOL[e]	100	0	-
9	0.54 mol% $[Ir(COD)Cl]_2$[f]	100	trace	-
10	0.54 mol% $[Ir(COD)Cl]_2$ +2 equiv. TPP[g]	100	8.6	16
11	0.54 mol% TPP-MOF-Ir[h]	100	50.7	94

[a]Reaction conditions: TPP-MOL-Ir catalyst (2.7 μmol Ir), 0.5 mmol of B_2pin_2, 2 mL of C_6H_5Cl, 24 h, other conditions as indicated. The $C_6H_4ClBpin$ was characterized by GC-MS. [b]Yield of $C_6H_4ClBpin$ was determined by ^{1}H-NMR based on B_2pin_2 conversion. [c]0.15 mmol of B_2pin_2 was

used as the boron source. [d]1 mmol of B_2pin_2 was used as the boron source. [e]TPP-MOL without $[Ir(COD)Cl]_2$ modification at an equal P quantity. [f]$[Ir(COD)Cl]_2$ dimer (2.7 μmol Ir) as the catalyst. [g]1 equiv. of $[Ir(COD)Cl]_2$ dimer and 2 equiv. of PPh_3 were added as the catalyst. [h]TPP-MOF-Ir (2.7 μmol Ir) catalyst.

C(sp^2)–H borylation of arenas with different electronic properties

Table S2 C(sp^2)–H borylation of arenas with different electronic properties by TPP-MOL-Ir catalyst.[a]

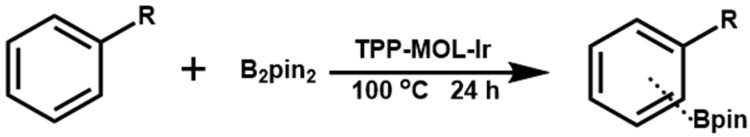

Entry	Arene	Product	Yield of C_6H_4RBpin(%)[b] *ortho: meta: para*	TON
1	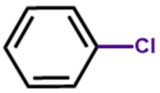	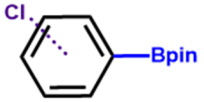	105.9 (1:0.78:0.31) 94.3 (1:1.06:0.45) 95.9 (1:1.31:0.59)	196 175 178
2	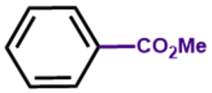	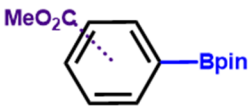	100.0 (1:0.15:0.08) 87.9 (1:0.10:0.06) 91.4 (1:0.11:0.07)	185 163 169
3		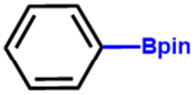	42.1 31.8 39.5	78 59 73
4	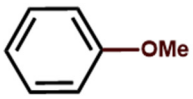	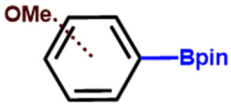	10.6 (1:2.09:1.30) 8.3 (1:2.38:1.12) 9.0 (1:2.29:1.37)	20 15 17
5	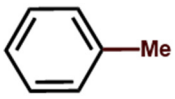	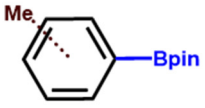	8.4 (1:0.30:0.21) 7.8 (1:0.32:0.18) 7.5 (1:0.32:0.18)	16 15 14

[a]Reaction Condition: TPP-MOL-Ir catalyst (0.54 mol% Ir), 0.5 mmol of B_2pin_2, 2 mL of arenes, 100 °C, 24h. Yield of C_6H_5Bpin and $C_6H_4CH_3(Bpin)$ were determined by GC-MS, other products were detected by ^{1}H-NMR.

10. Catalytic borylation of larger substrates

The TPP-MOL-Ir/TPP-MOF-Ir catalyst (3 μmol P, 0.54 mol% Ir), bis(pinacolate)diborane (B_2pin_2, 127 mg, 0.5 mmol), bis(2-ethylhexyl)phthalate (1.5 ml) or ethyl 3,4,5-trimethoxybenzoate (100 mg dissolved 1.5 ml THF) were added into a 25 ml schlenk tube in the glovebox. The reactants were gently stirred at 100 ℃ for 24 h. After cooling to room temperature, TPP-MOL-Ir/TPP-MOF-Ir was filtered by centrifugation and the supernatant was tested by ^{1}H-NMR (mesitylene as an internal standard) and GC-MS to determine the yield and selectivity for borylation product.

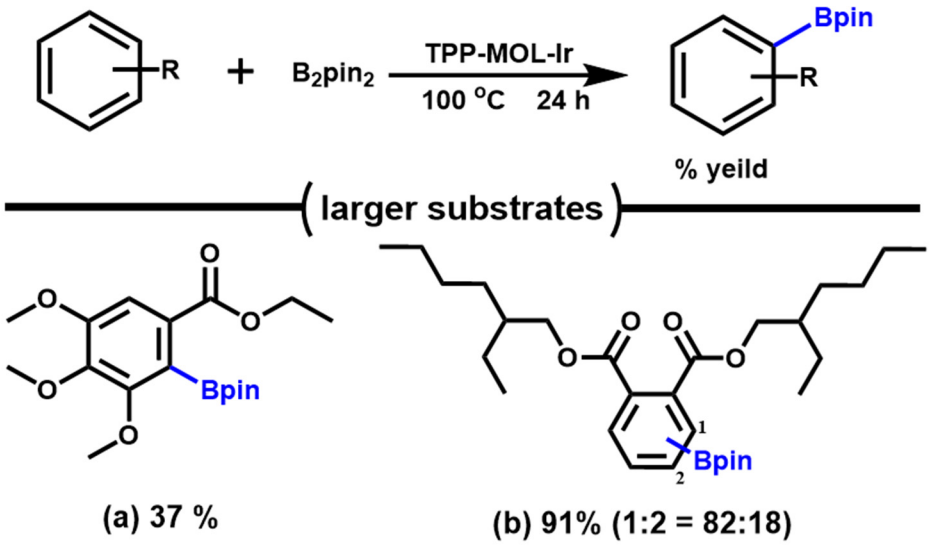

Fig. S16 Catalytic borylation of large substrates by TPP-MOL-Ir.

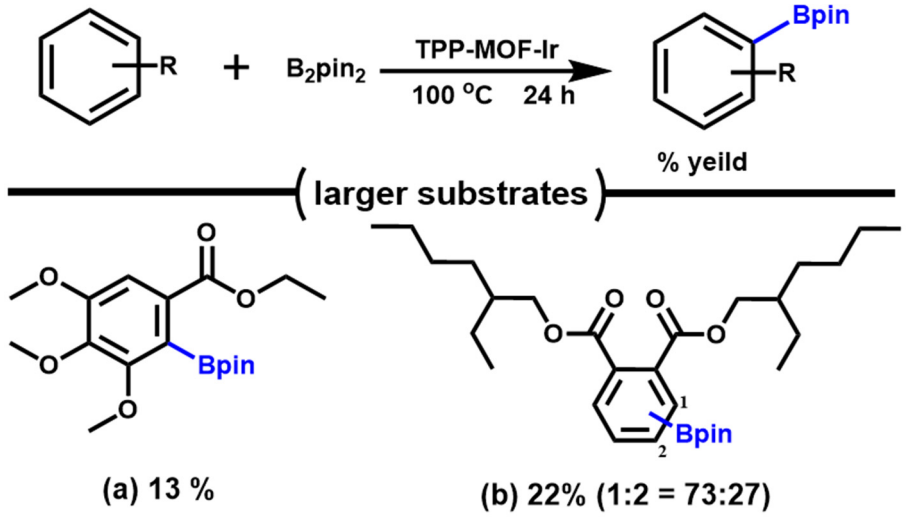

Fig. S17 Catalytic borylation of large substrates by TPP-MOF-Ir.

11. Testing the heterogeneity of TPP-MOL-Ir

As shown in Fig. S18, a hot filtration test was performed to eliminate the possibility of leached Ir species affecting the chlorobenzene borylation activity. TPP-MOL-Ir (0.54 mol% Ir) exhibited 99.5% yield in the first run. Then, the mixture was centrifuged in a glovebox, the separated supernatant was allowed to catalyze the reaction with freshly added B_2pin_2. The increase in yield (less than 1.6%) is negligible for the supernatant. The result confirmed that the actual catalytic species is MOL-supported mono(phosphine)-Ir complex as a heterogeneous catalyst, rather than any leached Ir species in the supernatant, which further demonstrated the heterogeneous nature for TPP-MOL-Ir catalysis.

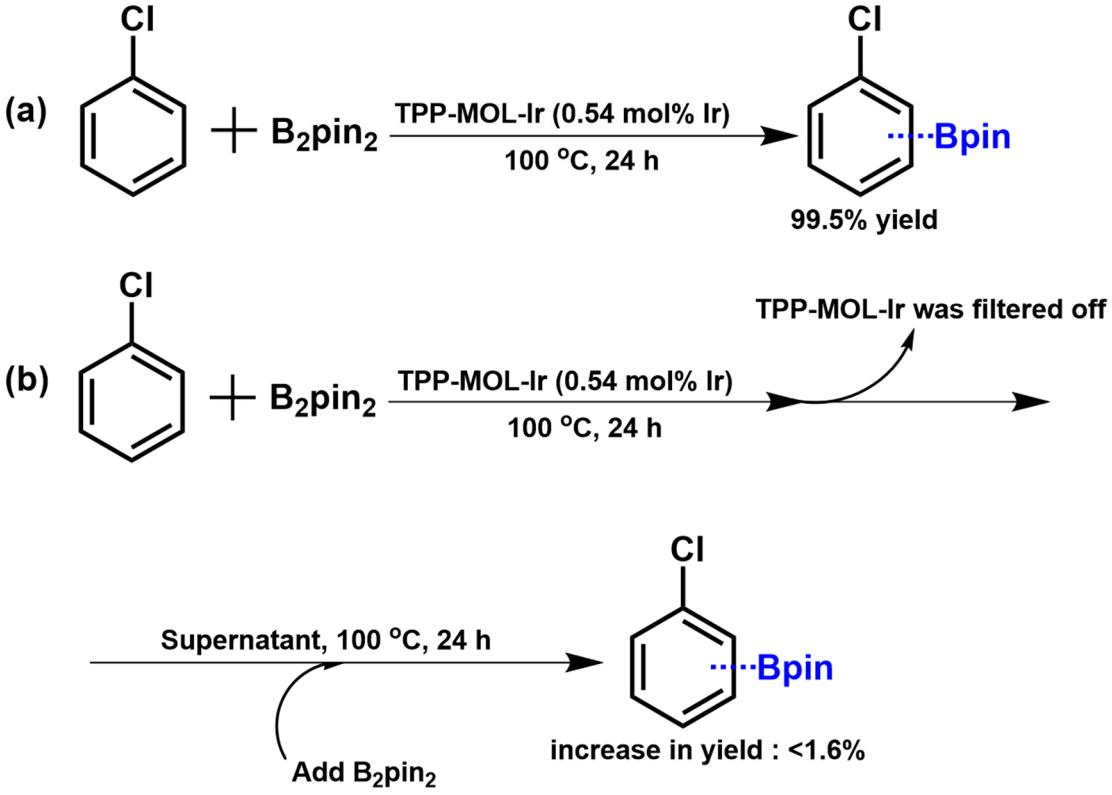

Fig. S18 Testing the heterogeneity of TPP-MOL-Ir via a hot filtration test. (a) TPP-MOL-Ir catalyst (0.54 mol% Ir), 0.5 mmol of B_2pin_2, 2 mL of chlorobenzene as a solvent, 100 °C, 24 h. (b) The separated supernatant as a catalyst.

12. Recycle of TPP-MOL-Ir catalyst

In a nitrogen-filled glovebox, TPP-MOL-Ir (8.1 μmol Ir), B_2pin_2 (25.4 mg, 0.1 mmol), and chlorobenzene (2 mL) were added into a 25 mL schlenk tube. After taking out of the glovebox, the reactor was stirred at 100 °C for 4 h. Under N_2 atmosphere, TPP-MOL-Ir catalyst was separated by centrifugation. The supernatant was tested by ^{1}H-NMR to access product yield using mesitylene as an internal standard. And the recovered MOL was wash with THF three times to be used for subsequent cycles of catalysis under the same condition. Yields: 1st cycle: 113.9%, 2nd cycle: 100.2%, 3rd cycle: 97.1%, 4th cycle: 65.0%, 5th cycle: 22.8%.

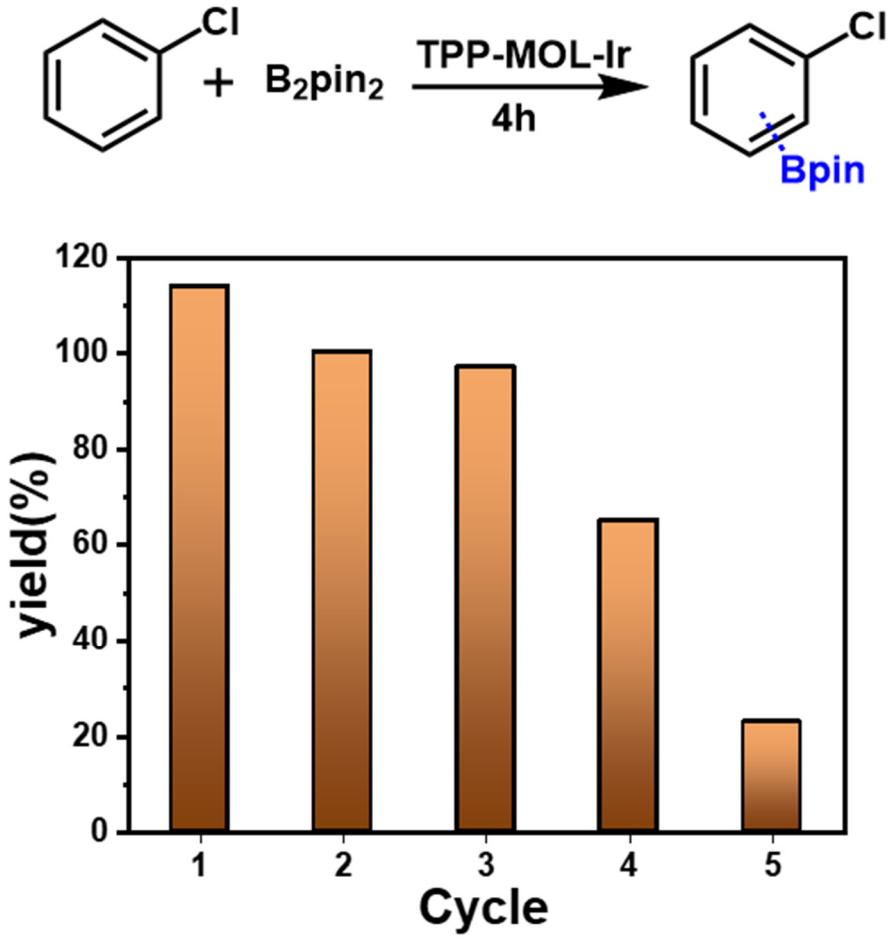

Fig. S19 Recycling of TPP-MOL-Ir catalyst for the C–H borylation of chlorobenzene.

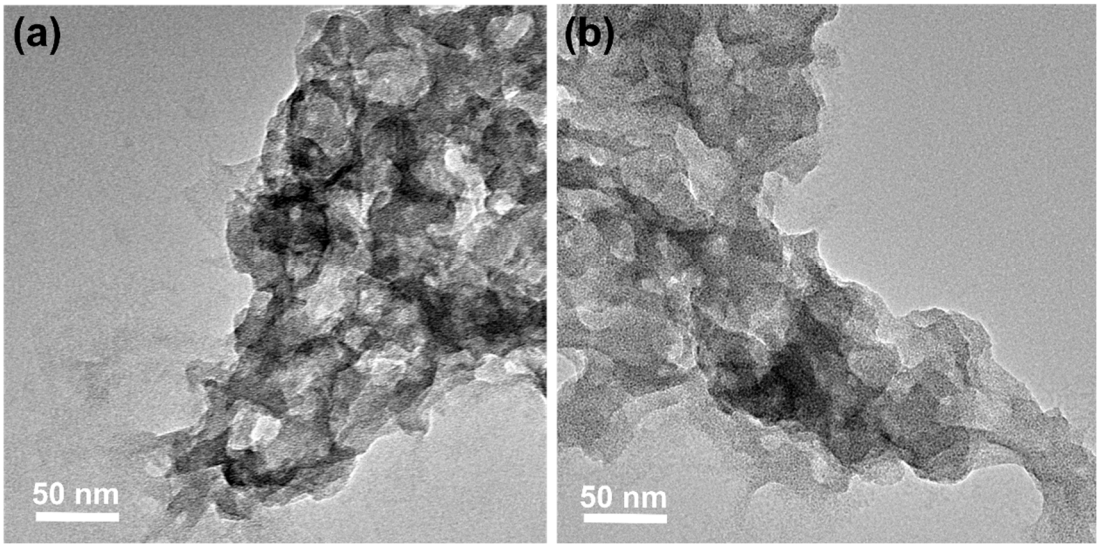

Fig. S20 (a, b) TEM images of TPP-MOL-Ir after the first and third run.

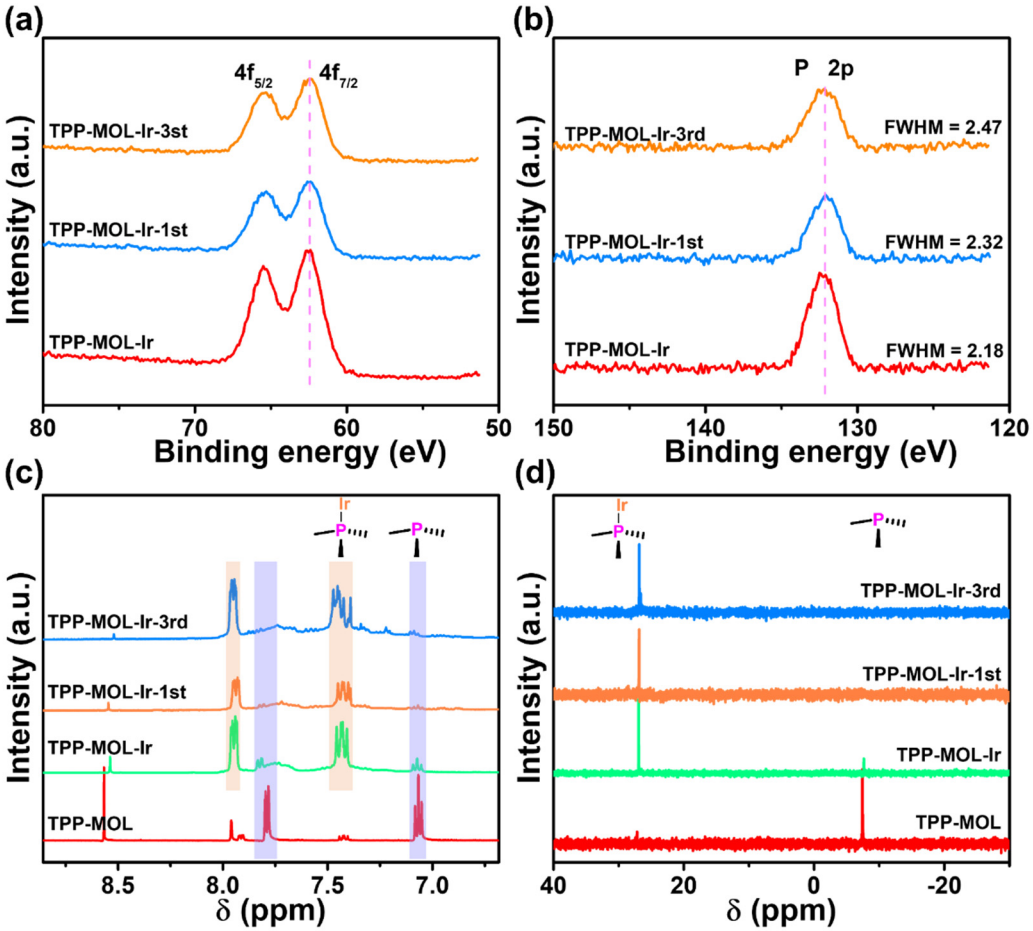

Fig. S21 XPS spectra in (a) Ir 4f and (b) P 2p region of the fresh TPP-MOL-Ir and the recovered TPP-MOL-Ir after the first and third run. (c) ^{1}H-NMR and (d) ^{31}P-NMR spectra of TPP-MOL, TPP-MOL-Ir and the recovered TPP-MOL-Ir after the first and third run.

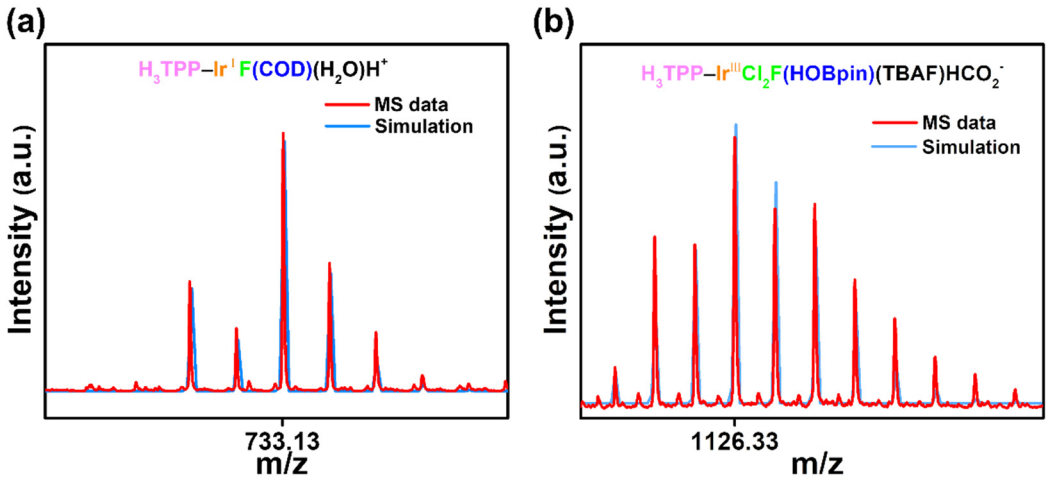

Fig. S22 (a) ESI-MS data of TPP-Ir^{I}-COD species in the TPP-MOL-Ir. Its formula is $(C_{21}H_{15}O_6)PIrF(C_8H_{12})(H_2O)H^+$ with the theoretical molecular weight of 733.13. (b) ESI-MS data of TPP-Ir^{III}-HOBpin species in the TPP-MOL-Ir after the borylation reaction. Its formula is $(C_{21}H_{15}O_6)PIrCl_2F(C_6H_{12}BO_2OH)[(C_4H_9)_4NF]HCOO^-$ with the theoretical molecular weight of 1126.34. The TPP-MOL-Ir sample first adopted a positive ion mode, and then the sample after reaction used a negative ion mode to effectively capture the signal considering that the system containing carboxylic acids. The HCO_2^- on the MOL, the TBAF for digestion and F^- introduced by it when the analysis of MS data.

13. Catalytic mechanism

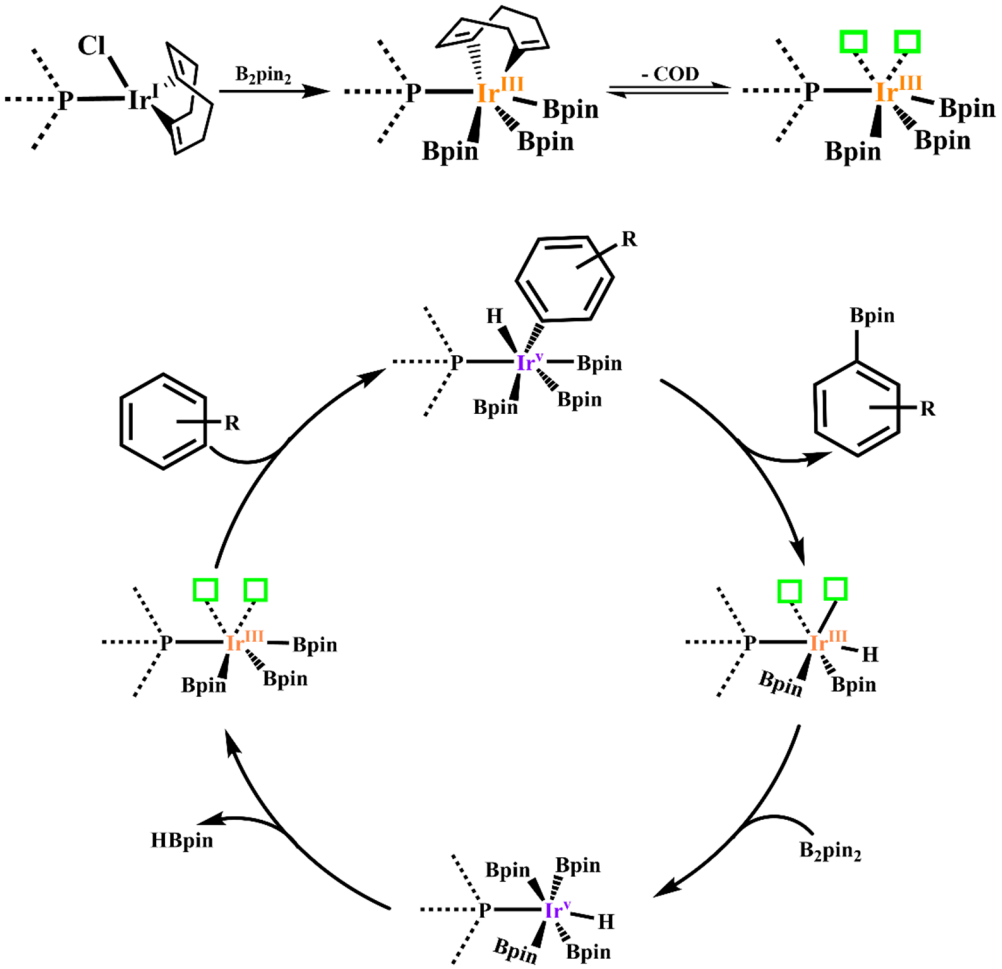

Fig. S23 Proposed catalytic cycle for arenes borylation catalyzed by P-$Ir^{III}(Bpin)_3$.

14. NMR spectra and GC chromatogram

The ^{1}H-NMR spectra were obtained by a short plug of silica gel, and the selectivity of the products were within the error range obtained from integral calculation in aromatic area region.

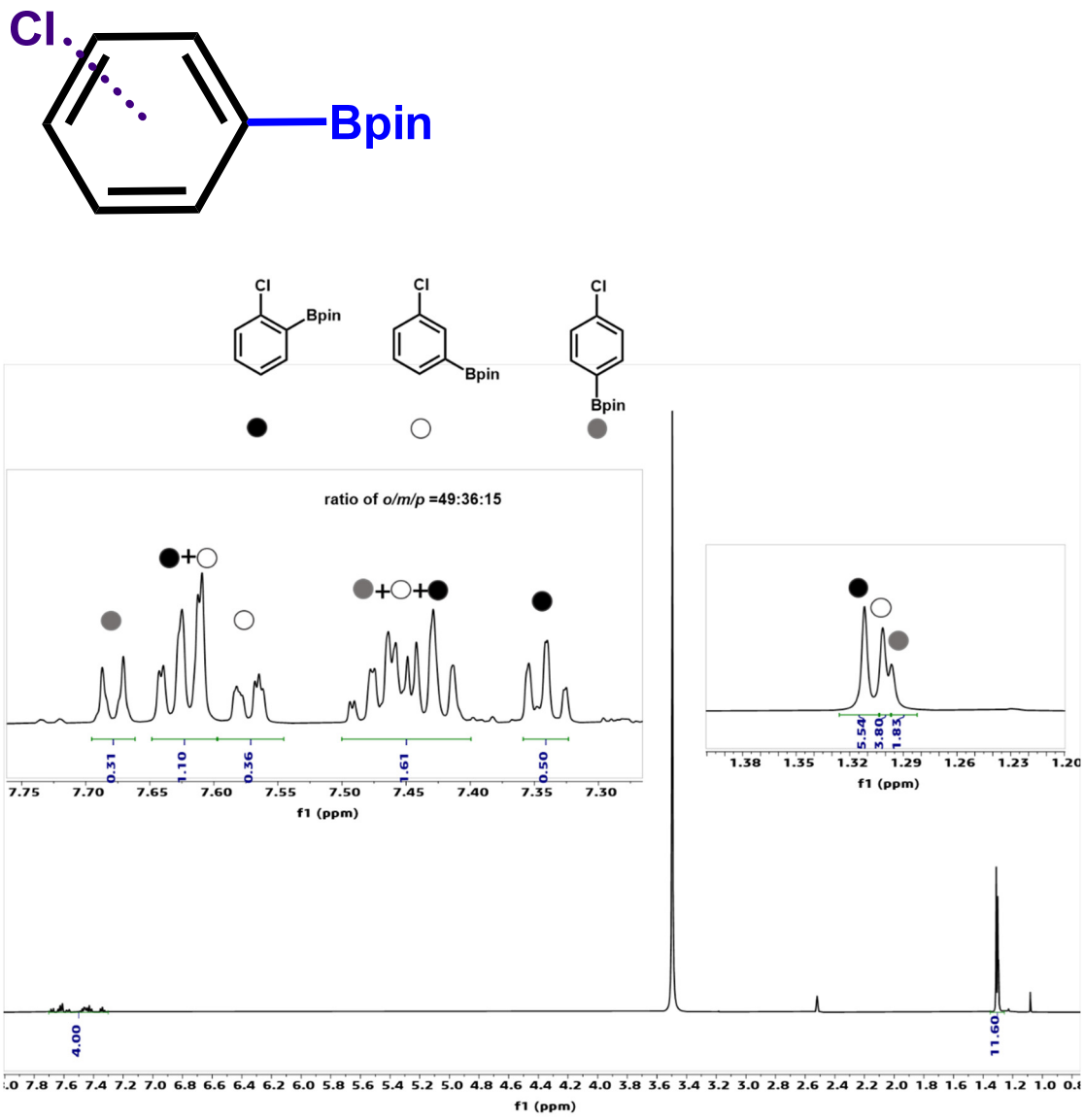

^{1}H-NMR (400 MHz, DMSO-d_6)

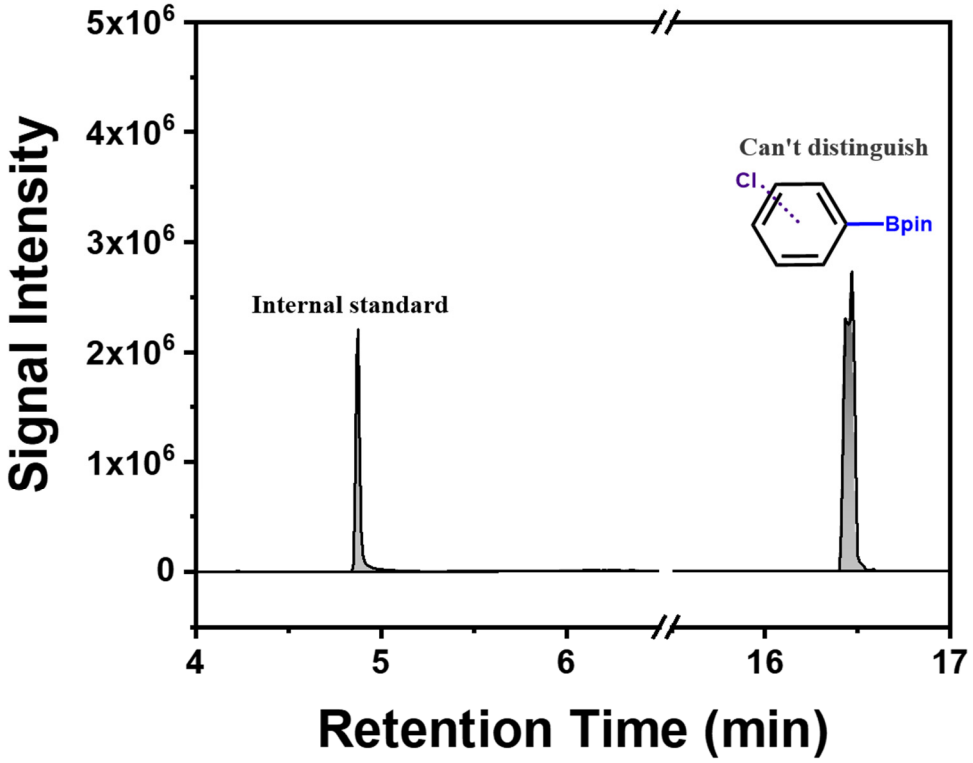

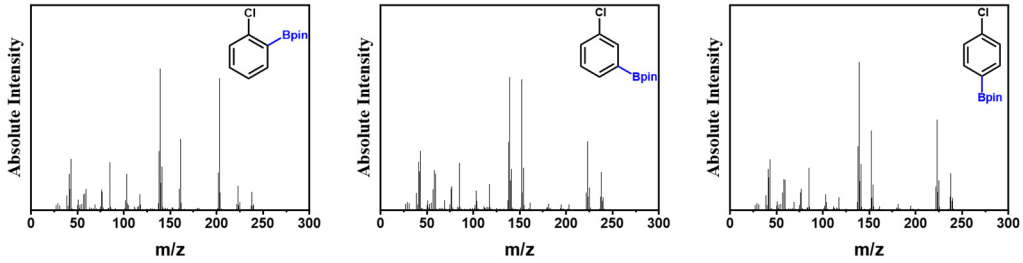

GC-MS Analysis

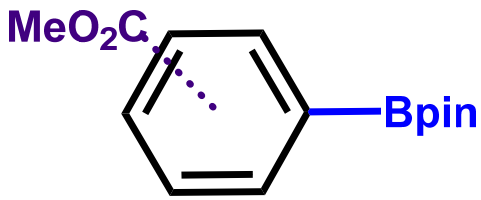

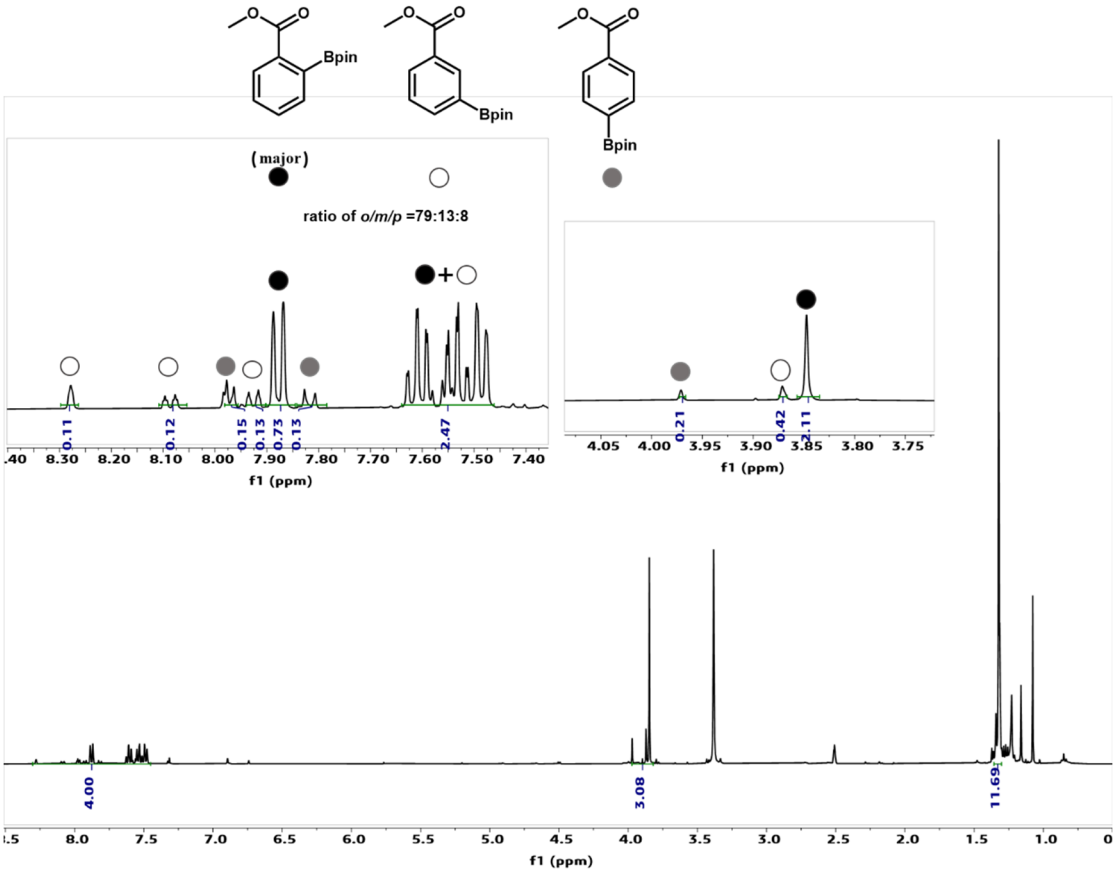

^{1}H-NMR (400 MHz, DMSO-d_6)

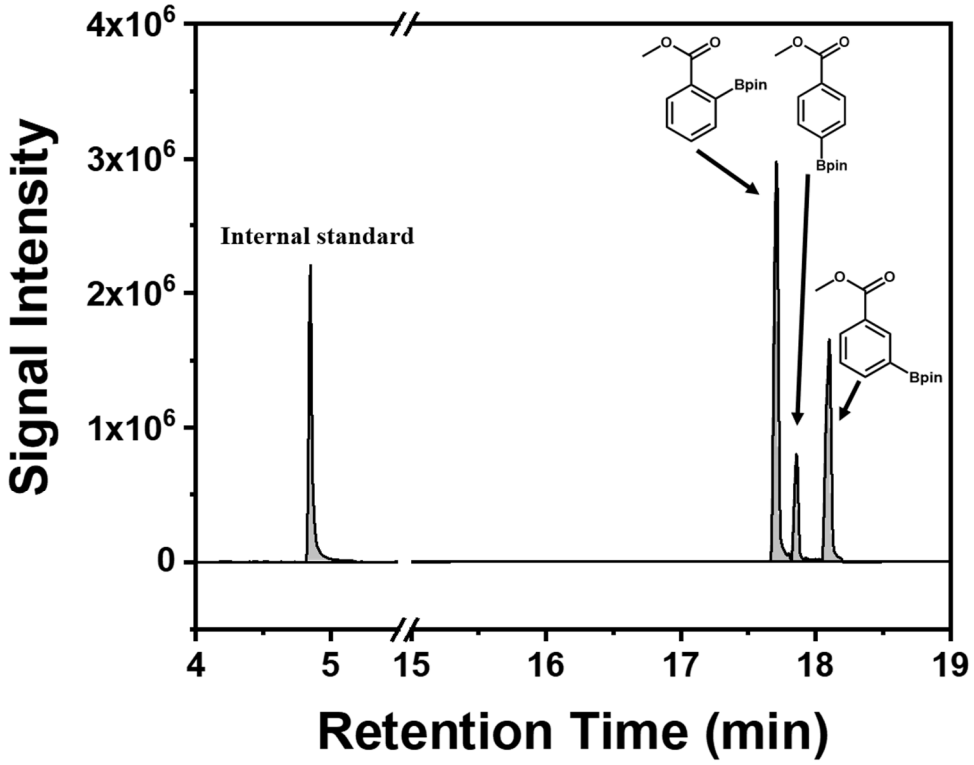

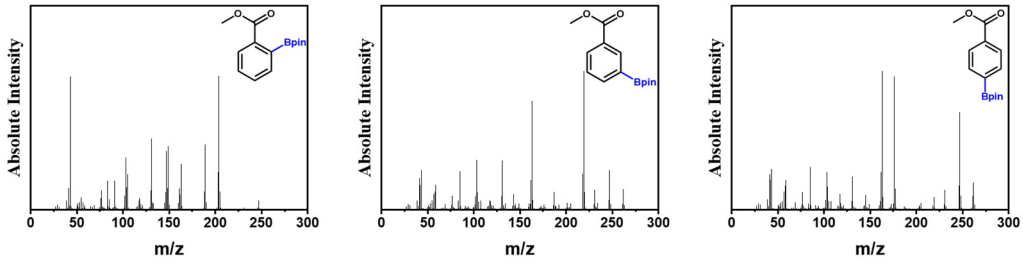

GC-MS Analysis

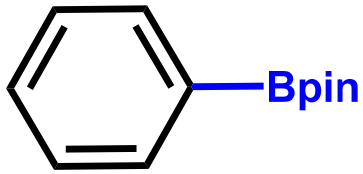

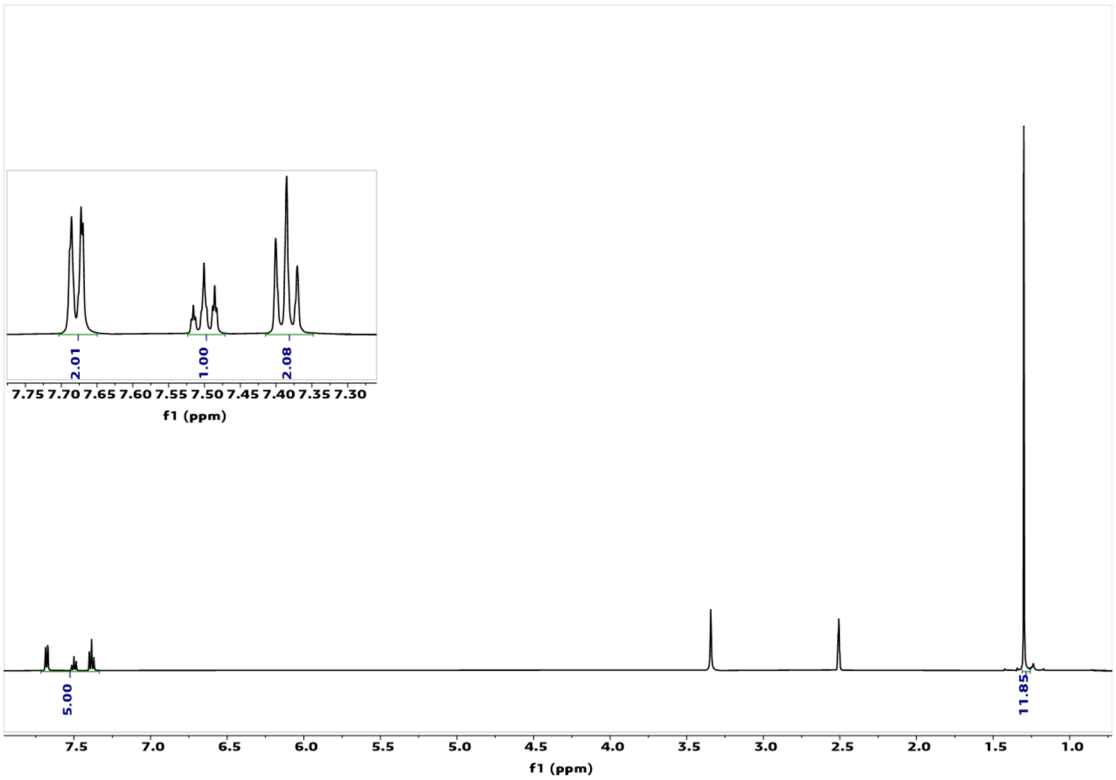

^{1}H-NMR (400 MHz, DMSO-d_6)

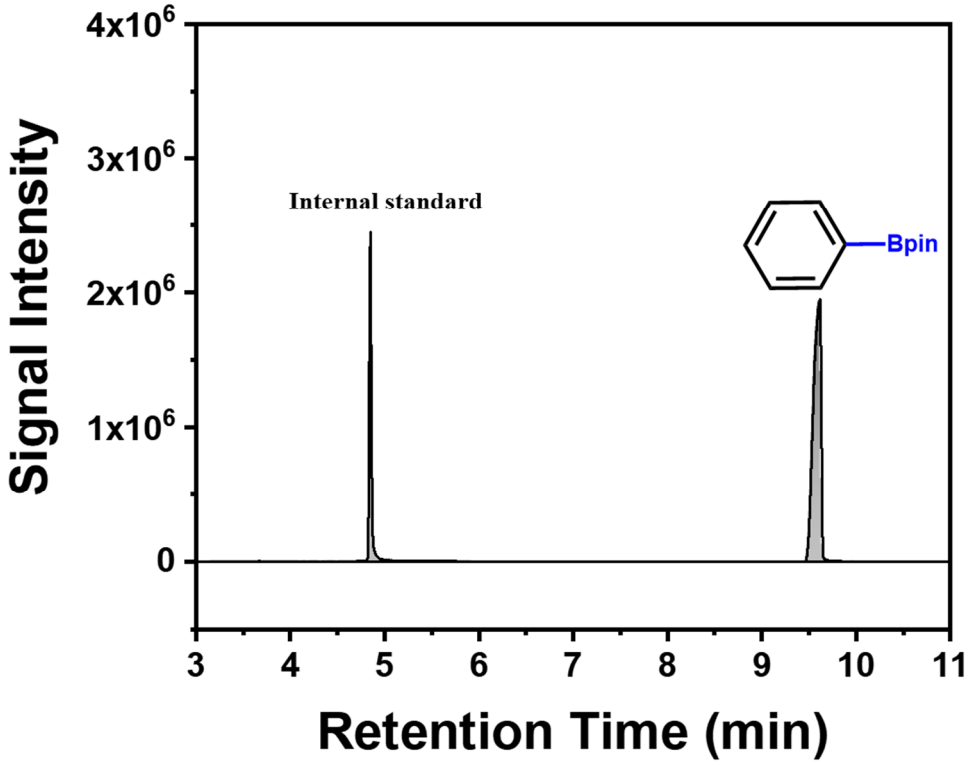

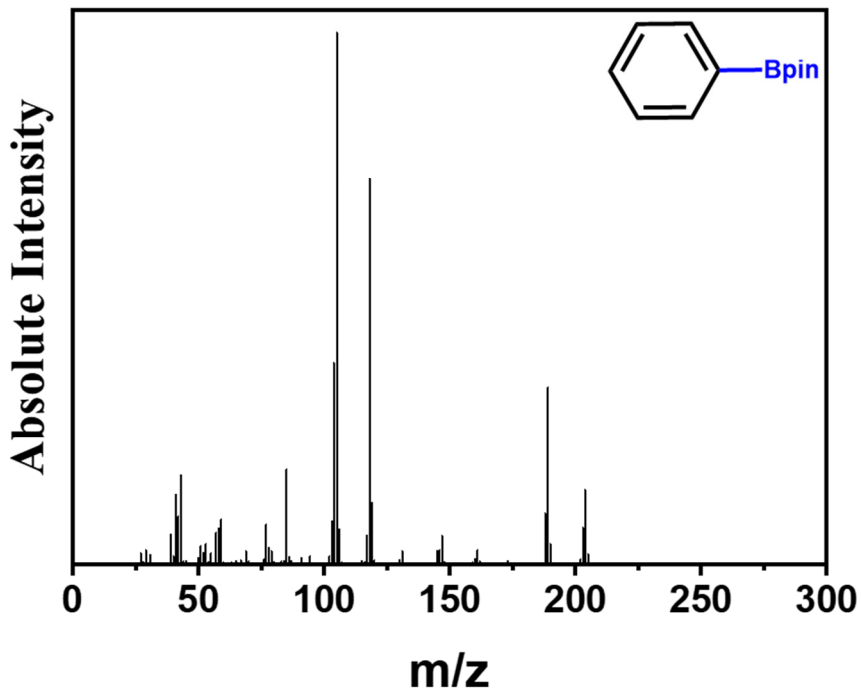

GC-MS Analysis

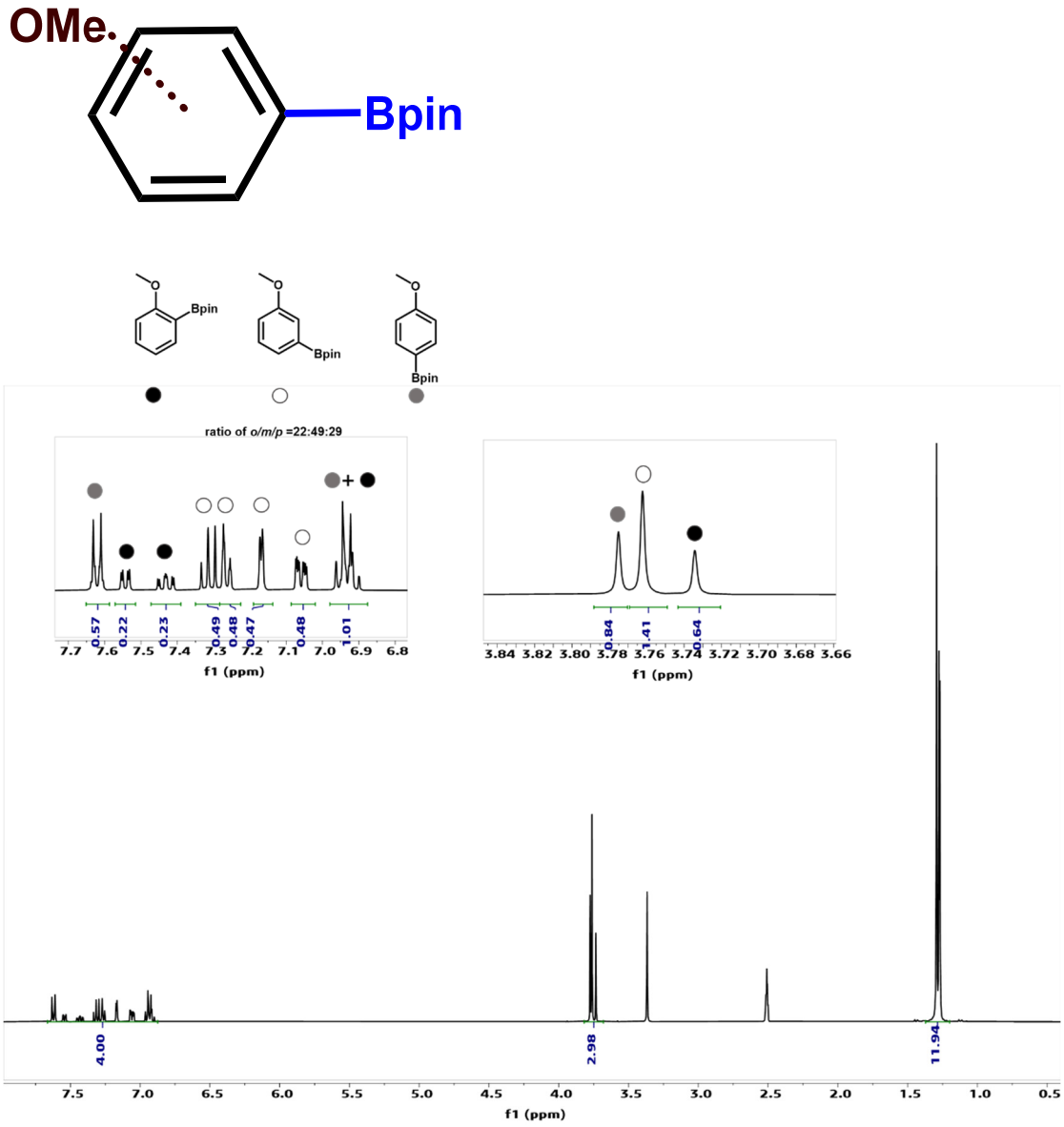

^{1}H-NMR (400 MHz, DMSO-d_6)

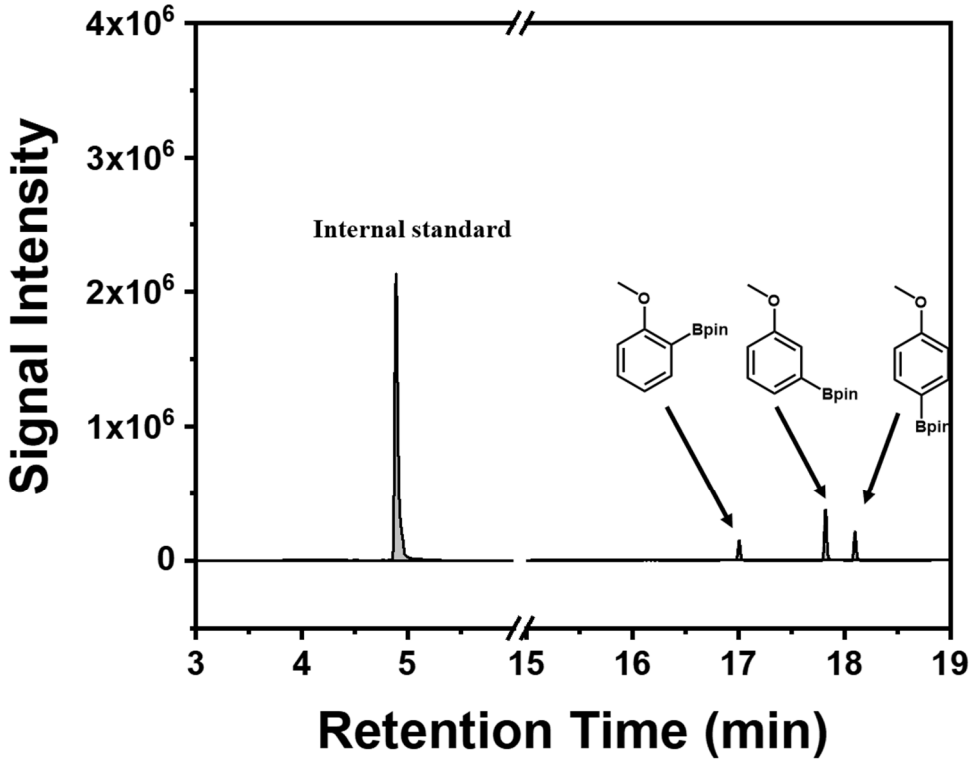

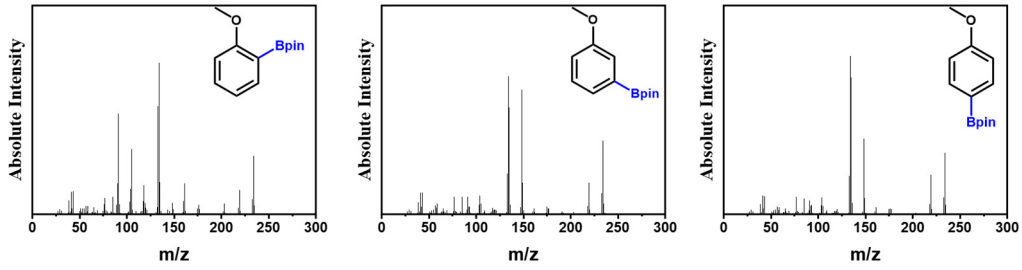

GC-MS Analysis

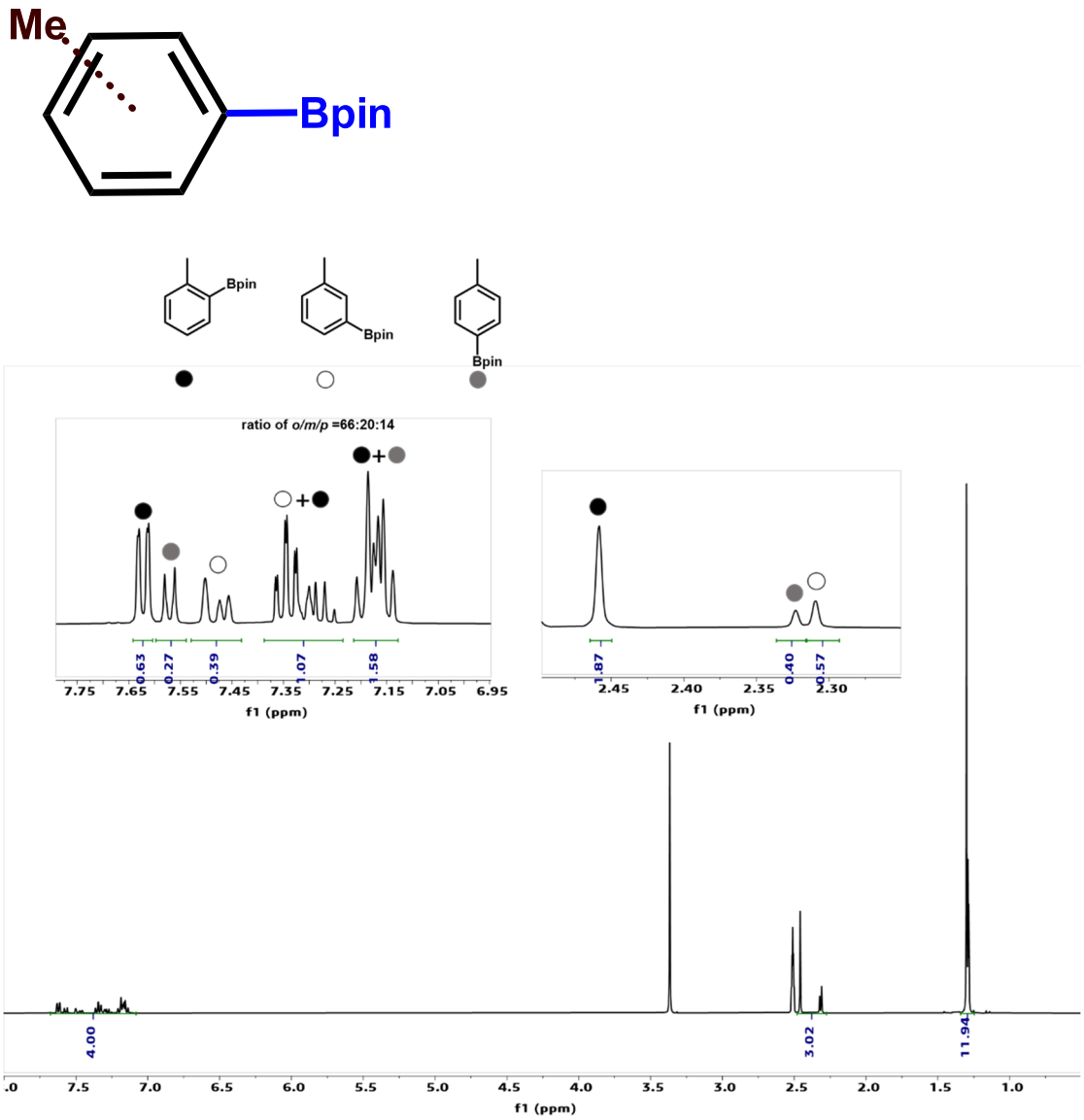

^{1}H-NMR (400 MHz, DMSO-d_6)

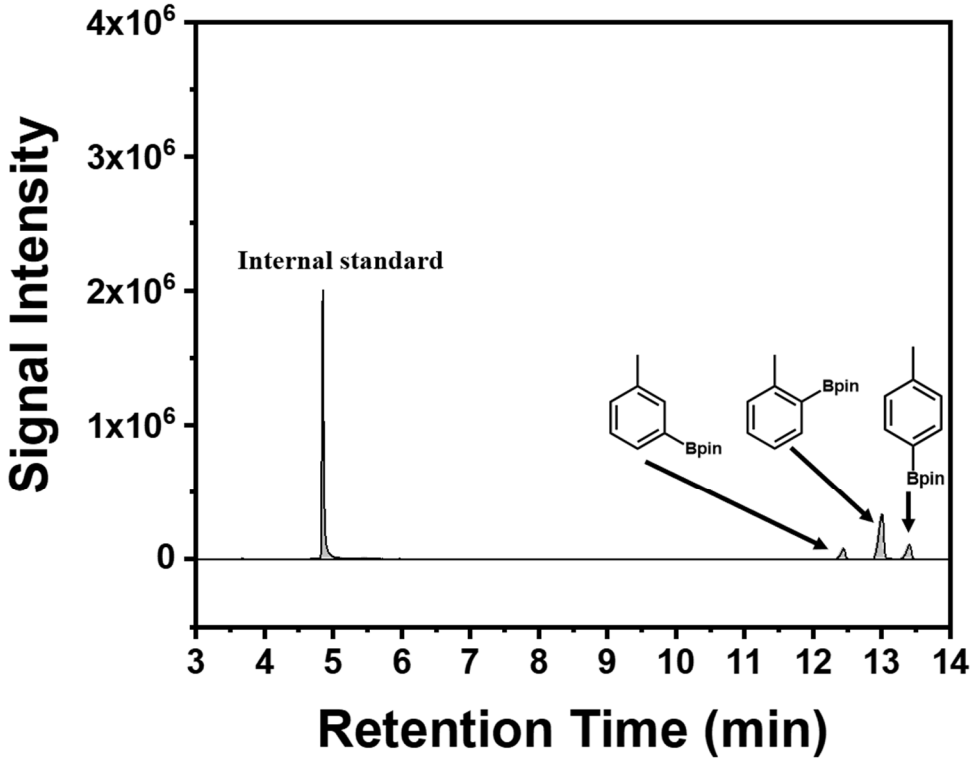

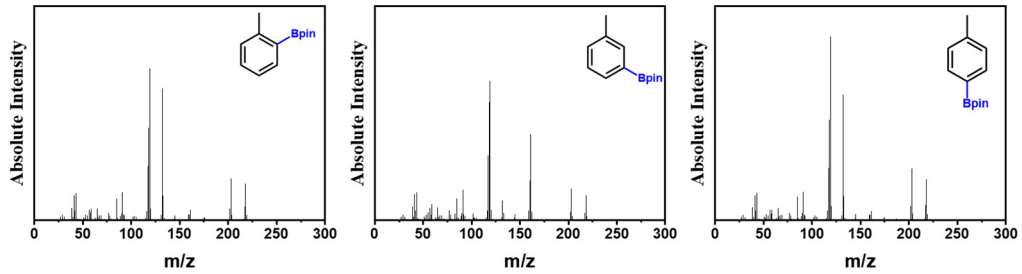

GC-MS Analysis

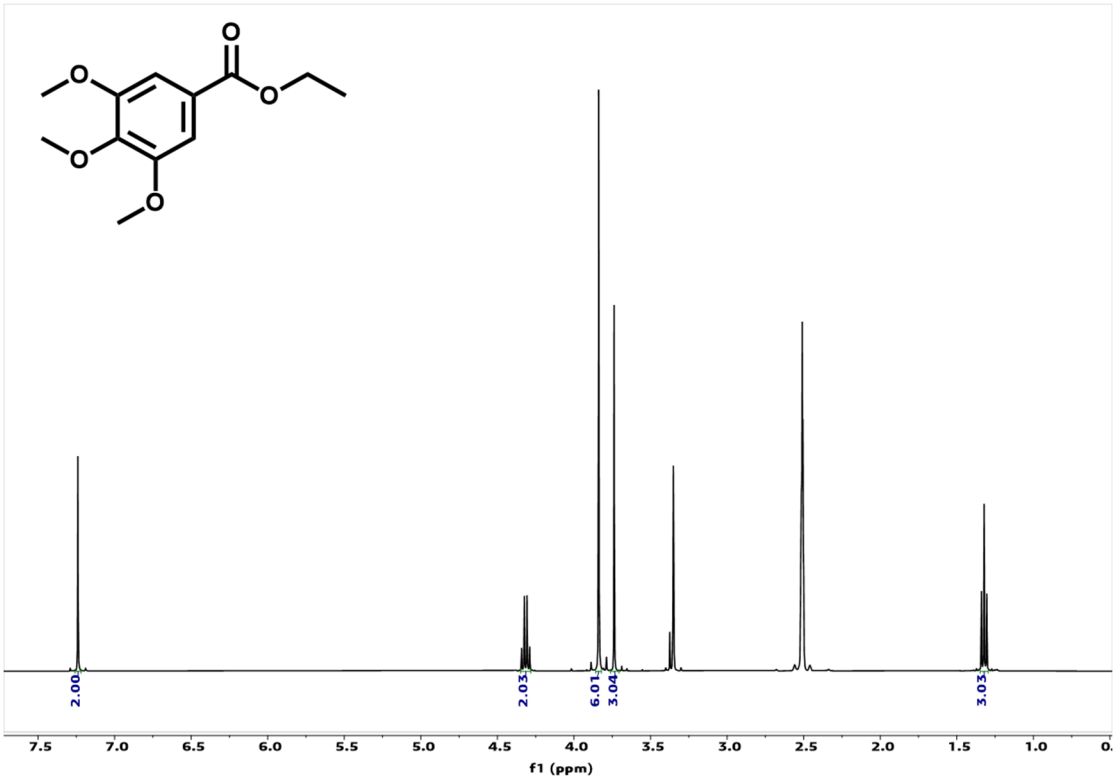

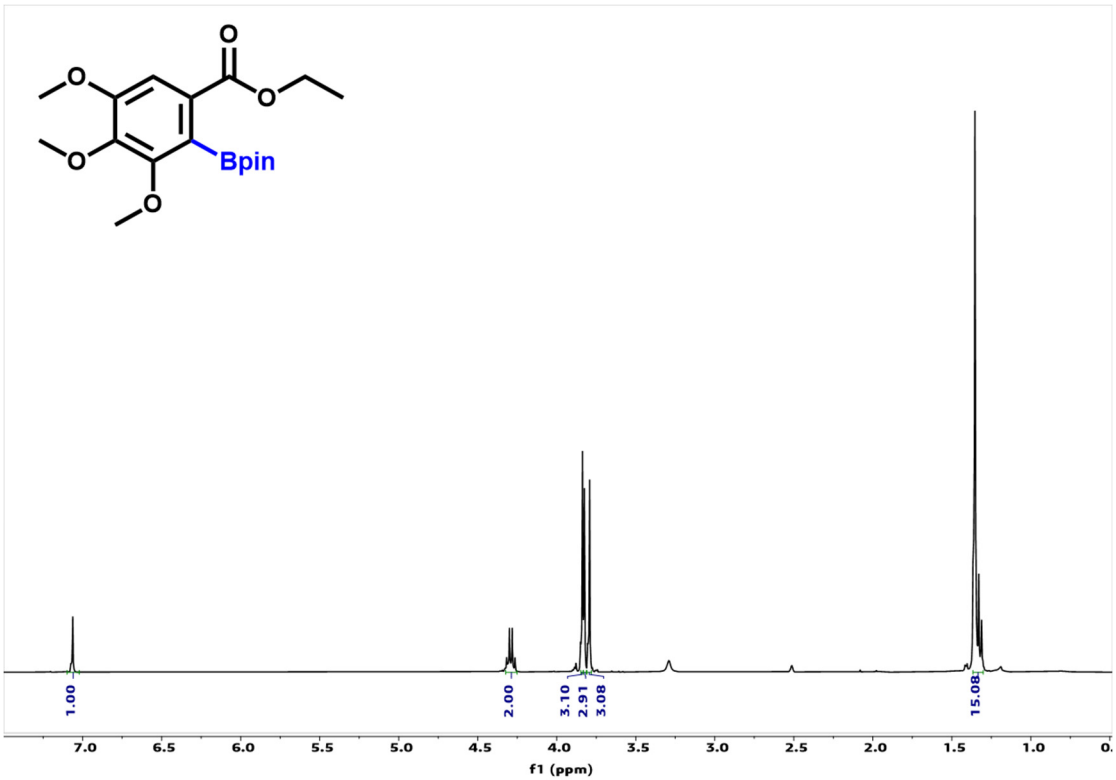

^{1}H-NMR (400 MHz, DMSO-d_6)

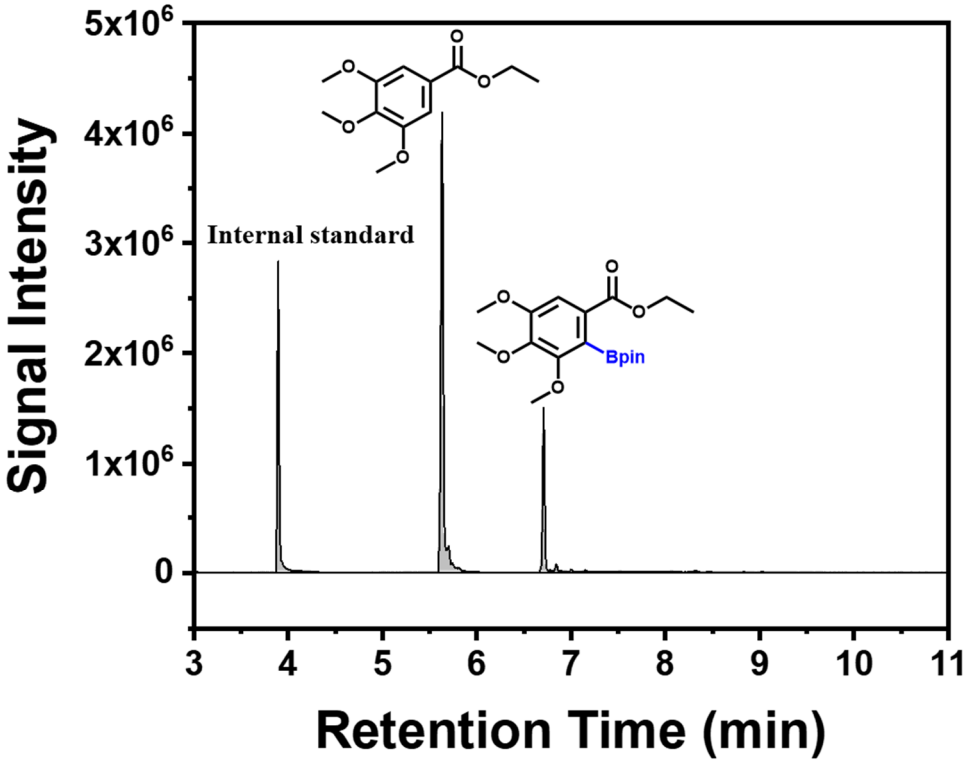

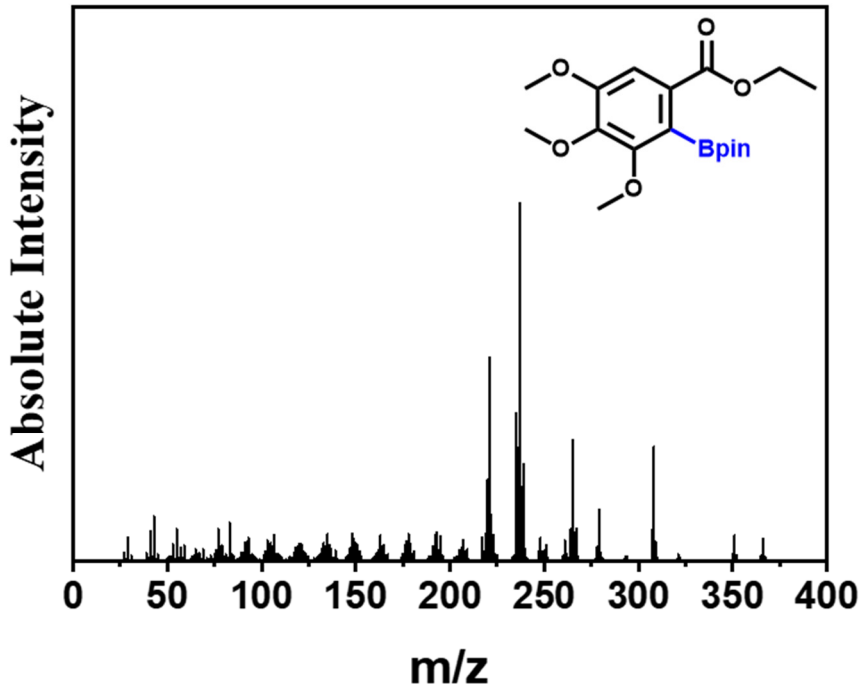

GC-MS Analysis

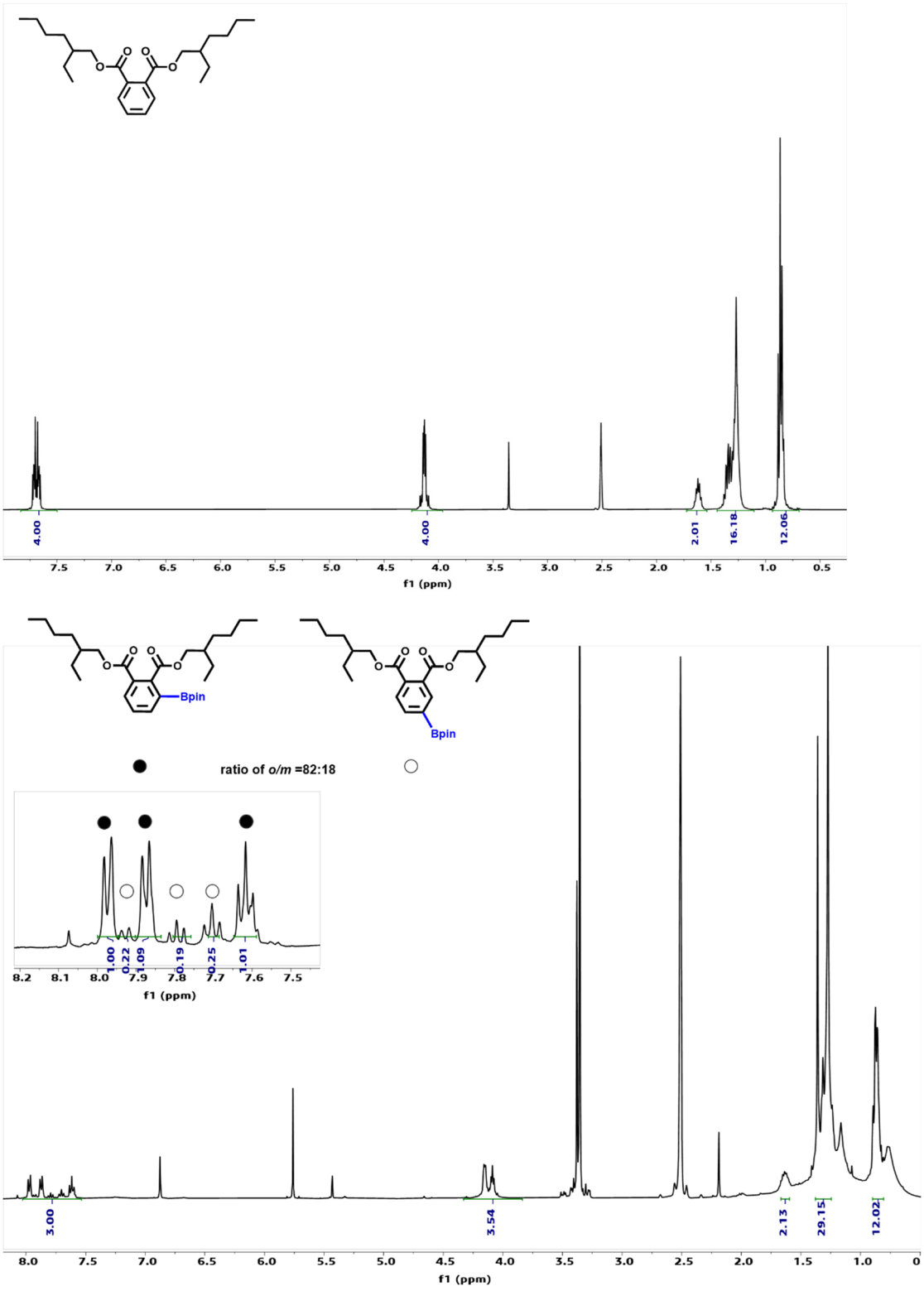

^{1}H-NMR (400 MHz, DMSO-d_6)

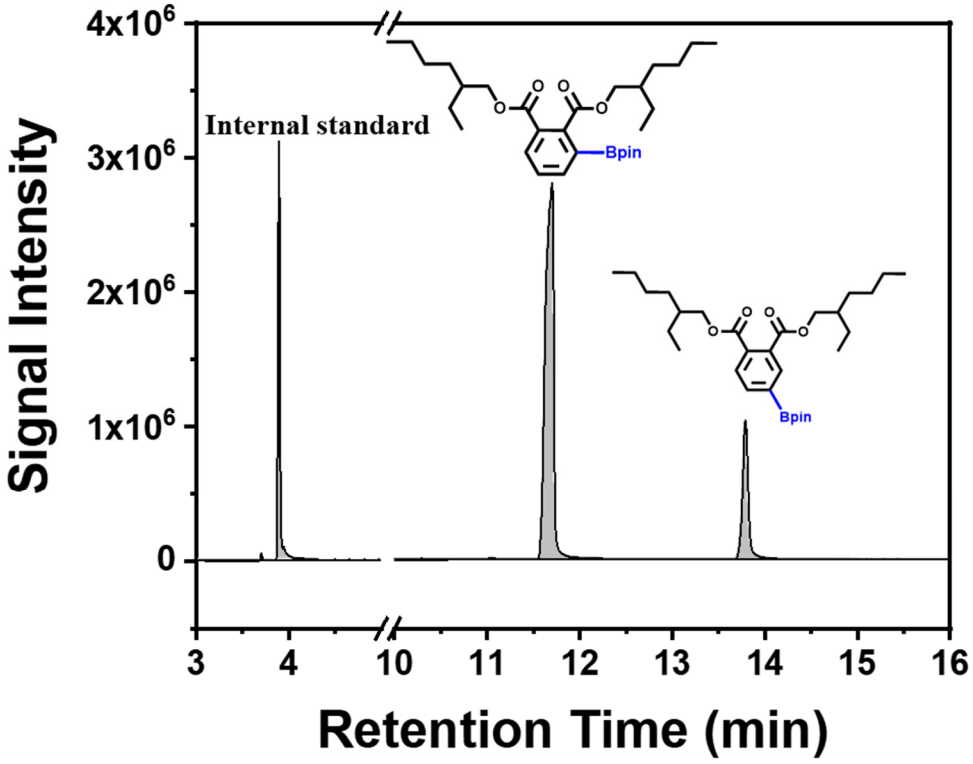

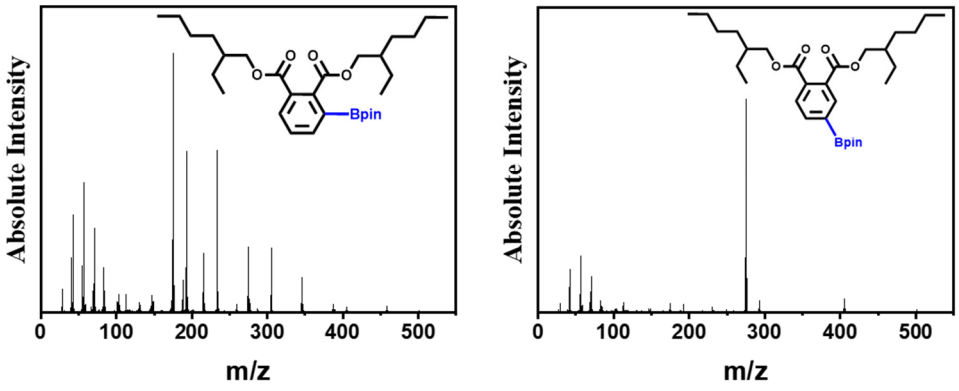

GC-MS Analysis

References

1. F. Däbritz, A. Jäger and I. Bauer, *Eur. J. Org. Chem.*, 2008, **2008**, 5571-5576.
2. T. G. Carroll, C. Hunt, R. Garwick, G. Wu, R. Dobrovetsky and G. Ménard, *Chem. Commun.*, 2019, **55**, 3761-3764.
3. L. Cao, Z. Lin, F. Peng, W. Wang, R. Huang, C. Wang, J. Yan, J. Liang, Z. Zhang, T. Zhang, L. Long, J. Sun and W. Lin, *Angew. Chem. Int. Ed.*, 2016, 55, 4962-4966.
4. Y. Jiang, L. Cao, X. Hu, Z. Ren, C. Zhang and C. Wang, *Inorg. Chem.*, 2018, **57**, 15123-15132.
5. M. Puchberger, F. R. Kogler, M. Jupa, S. Gross, H. Fric, G. Kickelbick and U. Schubert, Eur. *J. Inorg. Chem.*, 2006, **2006**, 3283-3293.
6. A. A. Bezrukov, K. W. Tornroos, E. Le Roux and P. D. C. Dietzel, *Chem. Commun.*, 2018, **54**, 2735-2738.
7. T. Sawano, Z. Lin, D. Boures, B. An, C. Wang and W. Lin, *J. Am. Chem. Soc.*, 2016, 138, 9783-9786.